A Dissertation for the Degree of Doctor of Philosophy in

Pharmaceutical Sciences

Anti-obesity effects of *Saururus chinensis* extract through enhancing energy expenditure

Department of Pharmacy

Graduate School

Chungnam National University

By

Ji-Hye Lee

Advisor **Sang Kyum Kim**

February 2018

Anti-obesity effects of *Saururus chinensis* extract through enhancing energy expenditure

Advisor Sang Kyum Kim

Submitted to the Graduate School
in Partial Fulfillment of the Requirements
for the Degree of
Doctor of Philosophy in Pharmaceutical Sciences

October, 2017

Department of Pharmacy

Graduate School

Chungnam National University

By

Ji-Hye Lee

To Approve the Submitted Dissertation

for the Degree of Doctor of Philosophy in Pharmaceutical Sciences

By Ji-Hye Lee

Title: Anti-obesity effects of *Saururus chinensis* extract through enhancing energy expenditure

December 2017

Committee Chair _____

Committee _____

Committee _____

Committee _____

Committee _____

Graduate School

Chungnam National University

CONTENTS

Materials and Methods

Results

List of Tables

List of Figures

List of abbreviations

WHO	World Health Organization
BMI	body mass index
WAT	white adipose tissue
BAT	brown adipose tissue
sWAT	subcutaneous adipose tissue
FFA	free fatty acids
ACC	acetyl-CoA carboxylase
FAS	fatty acid synthase
SREBP1	sterol regulatory element-binding protein 1
UCP	uncoupling protein
PGC	Peroxisome proliferator-activated receptor gamma coactivator
PRDM16	PR domain containing 16
NRF	nuclear respiratory factor
PPAR	Peroxisome proliferator-activated receptors
C/EBP	CCAAT/enhancer-binding protein
TFAM	mitochondrial transcription factor A
GLUT	Glucose transporter type
TNF	tumor necrosis factor
AMPK	AMP-activated protein kinase
pAMPK	Phospho-AMP-activated protein kinase
LKB1	Liver kinase B1

CaMKK β	Calcium/calmodulin-dependent protein kinase β
IBA	Immortalized brown adipocytes
S. chinensis	*Saururus chinensis*
SC	*Saururus chinensis* extract
T3	3,3’,5-Triiodo-L-thyronine
siAMPK	AMPKα1/2 siRNA
Dapi	4',6-diamidino-2-phenylindole
FDG	Fluorodeoxyglucose
PET/CT	Positron emission tomography/computed tomography
LFD	low-fat-diet
HFD	60% kcal fat-diet
LFD-Vehicle	LFD-fed mice treated with 0 mg/kg body weight SC
LFD-SC-100	LFD-fed mice treated with 100 mg/kg body weight SC
HFD-Vehicle	HFD-fed mice treated with 0 mg/kg body weight SC
HFD-SC-50	HFD-fed mice treated with 50 mg/kg body weight SC
HFD-SC-100	HFD-fed mice treated with 100 mg/kg body weight SC
AUC	Area under the curve
GTT	Glucose tolerance test
SCD-1	Stearoyl-CoA desaturase-1
ATGL	Adipose triglyceride lipase
HSL	Hormone-sensitive lipase
AST	Aspartate aminotransferase
ALT	Alanine aminotransferase
LDH	Lactate dehydrogenase

Introduction

1. Background

1.1 Obesity prevalence

The World Health Organization (WHO) defines obesity as abnormal or excessive fat accumulation that may impair health. Obesity is a major public health concern, as revealed by periodically assessed obesity rates. WHO weight classes categorized according to body mass index (BMI, weight [kg]/height [m^2]), a commonly used tool in epidemiological studies, are normal (BMI, 18.5–24.9), overweight (BMI, 25.0–29.9), and obese (BMI ≥ 30). In 2016, 39% of the world's adult population were overweight, and approximately 13% of the world's adult population were obese. Alarmingly, the worldwide obesity prevalence nearly tripled between 1975 and 2016. The OECD predicted that for obesity rates, BMI will continue to rise as a linear function of time in the OECD area (Figure 1). The increasing obesity prevalence is associated with serious health risks. Excessive fat accumulation is closely associated with insulin resistance and increased levels of pro-inflammatory factors, and obesity is associated with increased risk of nonalcoholic fatty liver disease, diabetes, hypertension, hyperlipidemia, cardiovascular disease, metabolic syndrome, and arthritis (Singla et al., 2010; Jung et al., 2014). Severe obesity (BMI, 35.0–39.9) or morbid obesity (BMI, 40–49.9) is not only associated with increased risk of disease and but also mortality (Abdelaal et al., 2017).

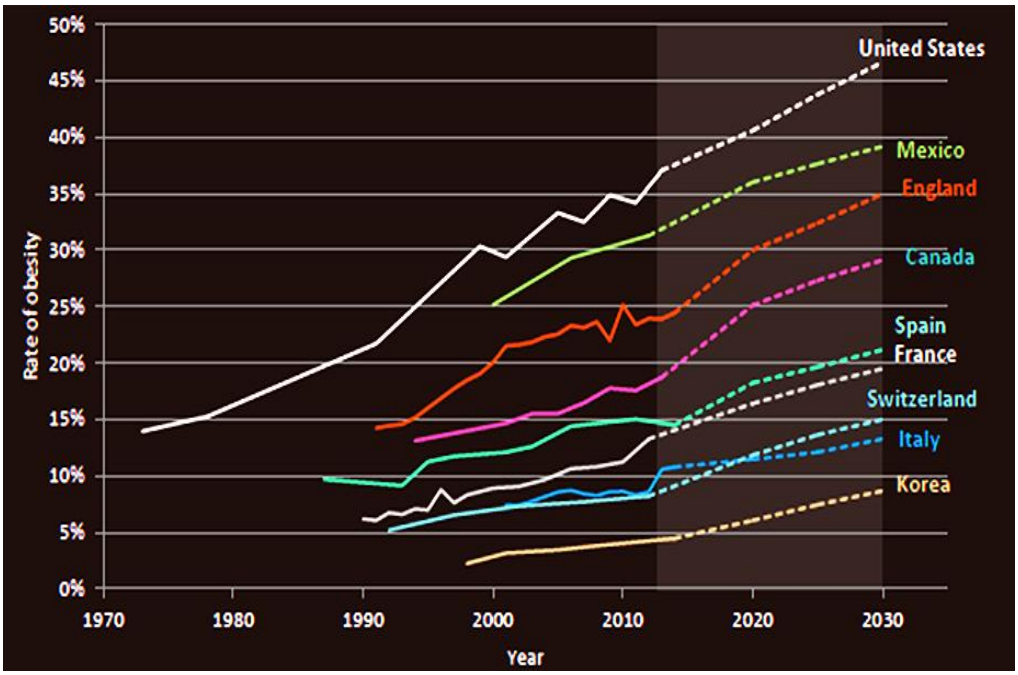

Figure 1. Projected rates of obesity (source: OECD, 2017).

1.2. Adipose tissue

1.2.1 Classification of adipose tissue

In addition to mostly mature adipocytes, adipose tissue also contains various cells including vascular endothelial cells, blood cells, fibroblasts, lipid precursors, macrophages, and other immune cells. Adipose tissue is found throughout the body and plays crucial roles such as energy storage, secretion of endocrine hormones and adipokines, protection of the body from external shock, and energy homeostasis (Coelho et al., 2013). Adipose tissue can be classified as white adipose tissue (WAT) or brown adipose tissue (BAT), based on location, function, and morphology. WAT is divided into visceral and subcutaneous fat compartments, depending on location. Visceral fat contains perirenal, omental, epicardial, retroperitoneal, mesenteric, and epithelial adipose tissue, and subcutaneous adipose tissue (sWAT) is mainly located below the skin in the abdominal, femoral, and gluteus areas (Luo L et al., 2016).

1.2.2. WAT

WAT formation begins before birth, but the size and number of adipocytes increase rapidly after birth and are known to affect diet composition (Gregoire et al., 1998). WAT is mostly composed of lipid droplet, and mitochondria are very rare. When insulin levels are increased by feeding, factors involved such as acetyl-CoA carboxylase (ACC), fatty acid synthase (FAS), and sterol regulatory element-binding protein 1 (SREBP1) are activated, and excess energy is stored as triglycerides in WAT (Wong et al., 2010). Excessive increase in WAT amount leads to the release of excess free fatty acids (FFA) into blood. Abnormally increased

FFA levels in turn inhibit binding of insulin to its receptor, insulin secretion, and insulin-mediated pathways and lead to hyperinsulinemia and elevated blood glucose levels (Terry et al., 1991).

WAT represents important endocrine organs and secrete hormones and cytokines. Representative adipokines include leptin, adiponectin, resistin, serpin, lipocalin-2, Pai-1, vaspin, visfatin, omentin, apelin, leptin, adiponectin, and pro-inflammatory cytokines. Leptin and adiponectin play a role in regulating energy metabolism and have been identified as useful indicators of insulin resistance (Inoue et al., 2005; Vazquez-Vela et al., 2008). WAT releases pro-inflammatory cytokines, such as tumor necrosis factor (TNF)-α, interleukin-6, and interleukin-1β (McArdle et al., 2013). Those pro-inflammatory cytokines promote release of further inflammatory mediator, and inflammatory signaling affects phosphorylation of insulin receptor substrate-1 and leads to insulin resistance and glucose uptake (Hotamisligil et al., 1995; Fasshauer et al., 2003; Jager et al., 2007; Fujisaka et al., 2009).

1.2.3. Brown adipose tissue

Compared with WAT, BAT has a very short history of research. Since the first official discovery of brown fat in 1902, the thermogenesis function in infants was reported in the 1960s that, and UCP1 was found in humans in the 1980s (Lee P et al., 2013). Primary brown preadipocytes have been reported to express a myogenic signature, myogenic factor 5, myoD, and myogenin (Timmons et al., 2007). The inhibition of myostatin (negative regulator of myogenesis) promotes adipogenesis in brown adipocyte not in white adipocyte (Zhang C et al., 2012). These

similarities in gene and protein expression between BAT and skeletal muscle demonstrate that the origin of BAT is distinct from WAT and close to skeletal muscle (Lee P et al., 2013). BAT has been reported to develop during embryogenesis. BAT is more prevalent in the body than WAT just before birth, but it decreases with age and is much less prevalent than WAT in adults. BAT was initially regarded as an organ that regulates body temperature through heat generation in babies and small animals. Conversely, development of advanced imaging technology has confirmed that BAT present in adults as well. BAT is located mainly in the supraclavicular and axillary areas (Cypess et al., 2009; van Marken Lichtenbelt et al., 2009; Virtanen et al., 2009). Whereas WAT stores energy as triglycerides, BAT consumes energy by generating heat. The characteristic brown color of BAT originates from the larger number of mitochondria than that found in WAT (Wu et al., 2013). Thermogenesis in BAT is activated by exposure to low temperatures, overfeeding, cardiac natriuretic peptides (Bordicchia et al., 2012), and some circulation stimulation, such as thyroid hormones (Guerra et al., 1996), BMP7 (Tseng et al., 2008), fibroblast growth factor-21 (Coskun et al., 2008), and retinoic acid (Puigserver et al., 1996). For instance, in cold exposure or overfeeding, signals transmitted to the brain lead to activation of the β-adrenergic system in BAT through an increase norepinephrine mediated by the sympathetic nervous system (SNS), with a subsequent increase in uncoupling protein (UCP) 1 expression and increase in body temperature (Figure 2) (Falcou et al., 1985; Trayhurn, 2017).

1.2.4 Beige adipocyte

A recent study reported that WAT expressed UCP1 (Cannon et al., 2004). The beige adipocyte (brown adipocyte-like white adipocytes) are derived from myogenic factor 5 negative precursors of inguinal WAT. Beige adipocyte is derived from WAT, but the function is similar to BAT. Beige adipocyte has more mitochondria, fatty acid oxidation, and respiratory chain than WAT, and beige adipocyte generates heat through UCP1 expression, which increases energy consumption (Lizcano et al., 2016). Browning of WAT has been shown to be stimulated by hormonal interplay and numerous environmental factors. For example, conversion of WAT to beige adipocytes has been shown to occur because of cold exposure or in response to β-adrenergic and Peroxisome proliferator-activated receptor (PPAR) γ agonist treatment (Wu et al., 2013). Exercise has also been reported to increase WAT browning and energy expenditure (Cui et al., 2016). Furthermore, UCP1 and other thermogenic components have been shown to associate with WAT browning. Several studies have investigated factors associated with thermogenesis and mitochondrial biogenesis and their role in obesity.

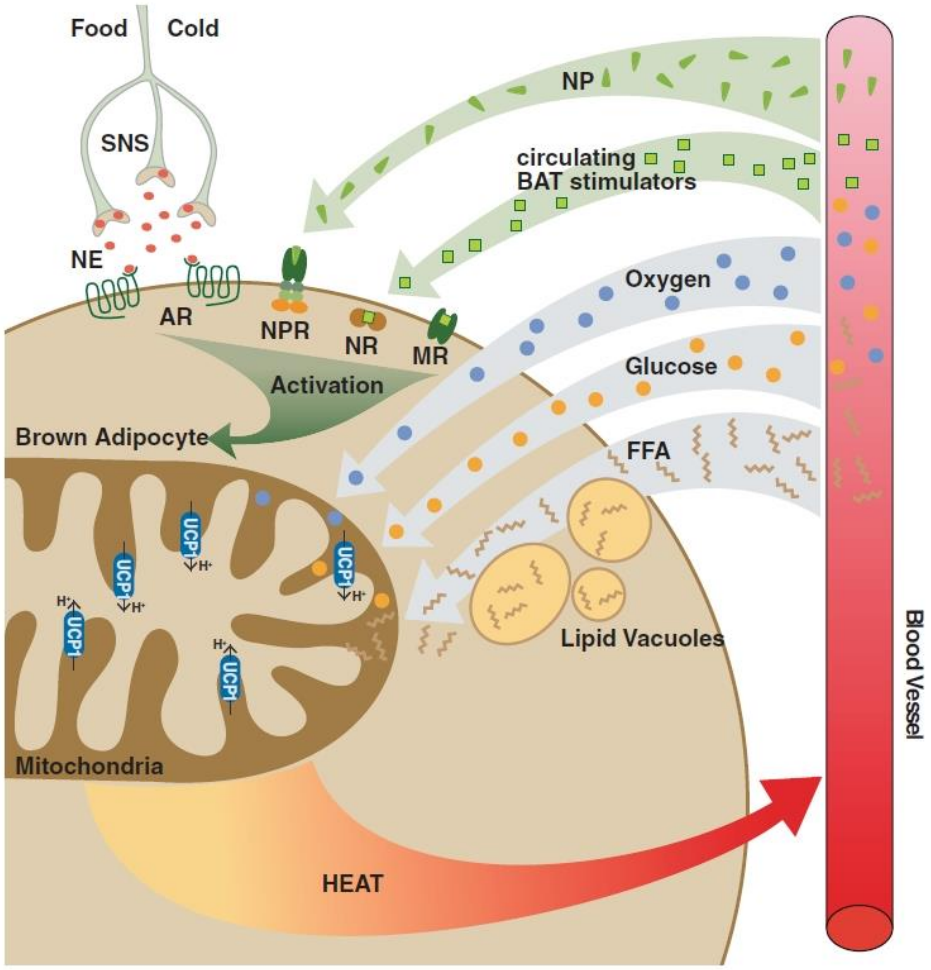

Figure 2. Activation of brown adipose tissue (Thoonen et al., 2016).

H+, proton; FFA, free fatty acids; UCP1, uncoupling protein 1, SNS, sympathetic nervous system; NE, norepinephrine; AR, adrenergic receptors; NPR, natriuretic peptide receptors; NP, natriuretic peptides; NR, nuclear receptors; BAT, brown adipose tissue; MR, membrane receptors.

1.3 Thermogenic factor

1.3.1 UCP1

UCPs are members of the mitochondrial carrier protein family, located in inner mitochondrial membrane. Members of the UCP family share structural similarities but differ in their tissue expression patterns among mammals. Although UPC2 is widely distributed throughout the body, UCP3 is restricted to the skeletal muscle, and UCP4 and UPC5 are expressed in brain. UCP1, also known as thermogenin or SLC25A7, is expressed primarily in BAT (Brondani et al., 2012).

H^+, produced in the electron transfer system, is involved in ATP production as part of a process called coupling. UCP1 is uncoupled from H^+ entering mitochondria and ATP synthesis, because H^+ ion enters the intracellular mitochondria and releases energy in the form of heat without synthesizing ATP (Dalgaard et al., 2001). UCP1 expression is activated by nonesterified fatty acids and inhibited by purine nucleotides (i.e., GDP, ATP, and ADP) (Brondani et al., 2012).

1.3.2 PGC1α

Peroxisome proliferator-activated receptor gamma coactivator (PGC)1α is a transcription coactivator that interacts with a broad range of transcription factors that are involved in a wide variety of biological responses such as adaptive thermogenesis, mitochondrial biogenesis, and glucose/fatty acid metabolism (Puigserver et al., 1998; Wu et al., 1999). PGC1α is expressed at high levels in tissues where mitochondria are abundant and oxidative metabolism is active.

PGC1α is known to increase in cold exposure and contributes to thermogenesis. Increased PGC1α induces transcription of nuclear respiratory factor (NRF)1 and NRF2, leading to increased expression of mitochondrial transcription factor A (TFAM), which translocate to the mitochondria to stimulate mitochondrial biogenesis as manifested by increased mitochondrial DNA replication and mitochondrial gene expression. PGC1α also interacts with another nuclear hormone receptor, PPARα, to enhance UCP1 expression (Liang and Ward, 2006).

1.3.3 PR domain containing 16

PR domain containing 16 (PRDM16) is a key transcriptional co-regulator that controls the development of brown adipocytes in BAT and an indispensable transcriptional factor that specifies the brown adipocyte identity. shRNA-mediated depletion of PRMD16 was demonstrated to cause a decrease in the expression of thermogenic genes such as UCP1, PGC1α, and cytochrome c oxidase subunit 8b as well as a reduction in uncoupled cellular respiration (Seale et al., 2011). Hormones and cytokines, including T3, NE, BMP7, FGF21, and NP can regulate brown adipogenesis by altering PRDM16 expression (Villanueva et al., 2013). In addition to its function as a brown adipose determination factor, PRDM16 also contributes to brown fat-like gene programming and thermogenesis in sWAT (Seale et al., 2011).

1.4 AMP-activated protein kinase

1.4.1 The structure of AMPK

AMP-activated protein kinase (AMPK) is a heterotrimeric complex consisting of two catalytic α subunits (α1 and α2, 63 kDa), two scaffolding β subunits (β1 and β2, 40 kDa), and a regulatory γ subunit (38 kDa, composed of γ1, γ2, and γ3) (Stapleton et al., 1997). These different subunits can be arranged in 12 distinct trimeric (αβγ) complexes. The catalytic site of AMPK is located at the N-terminal of α subunit, and phosphorylation of threonine 172 (Thr172) within this site leads to kinase activation (Hawley et al., 1996). Therefore, AMPK activation is assessed using a phosphorylated antibody against Thr172 of AMPK in most studies. Given that most of the physiological actions of AMPK are ascribed to the catalytic site of α subunit, understanding the distribution of α subunits is important. Among the two currently known catalytic site isoforms, α1 is widely distributed throughout the body, whereas α2 is mainly expressed in skeletal muscle, heart, liver, and kidney (Stapleton et al., 1996). C-terminus of α subunit contains a site that binds β and γ subunits. The β subunit has a glycogen-binding domain that has been reported to detect changes in glycogen structure (Hudson et al., 2003), whereas the γ subunit has AMP/ATP binding sites for detection of energy levels (Scott et al., 2004; Towler et al., 2007).

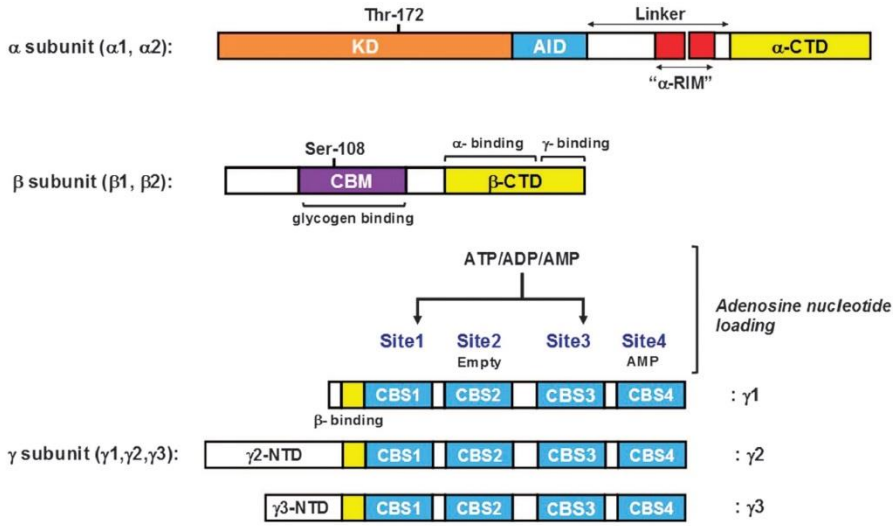

Figure 3. Functional domains of AMPK subunits (Kim J et al., 2016).

KD, kinase domain; AID, auto inhibitory domain; CTD, C-terminal domain; CBM, carbohydrate binding module; CBS, cystathione-β-synthases domain.

1.4.2 The role of AMPK activation

AMPK is a known regulator of lipid and glucose metabolism and plays an important regulatory role in diabetes and obesity (Towler et al., 2007). Once activated, AMPK induces a catabolic reaction to increase ATP production and suppress an anabolic reaction to decrease ATP consumption. ACC is a key enzyme of the lipogenic pathway and catalyzes malonyl-CoA synthesis from acetyl-CoA (Park et al., 2002). ACC inactivation leads to a decrease in malonyl-CoA, which in turn leads to a decrease in FAS and stearoyl-CoA desaturase-1 expression. Several *in vivo* and *in vitro* studies have demonstrated phosphorylation of ACC by AMPK. Activation of AMPK in adipocytes leads directly to ACC phosphorylation, which contributes to decreased body weight and fat mass by inhibiting lipogenic rate affects (Sullivan et al., 1994). Decreased malonyl-CoA leads to fatty acid oxidation, alleviating the inhibition on carnitine palmitoyltransferase (CPT) 1, which catalyzes the entry of fatty acids to mitochondria as the rate-limiting enzyme for fatty acid oxidation (Matejkova et al., 2004). AMPK is activated by signal transduction and intracellular stress responses that increase the AMP/ATP ratio, such as hypoglycemia, extreme exercise, hypoxia, and hypothermia, and it is generally not activated under normal circumstances. Maintenance of energy homeostasis forms the basis for various AMPK-mediated changes in biological functions. AMPK is also closely related to energy consumption through thermogenesis. Hypothalamic AMPK activation regulates BAT thermogenesis via the sympathetic nervous system (Lopez et al., 2017). Several lines of evidence indicate that T3, estradiol, and nicotine regulate energy expenditure through downregulation of hypothalamic AMPK activity (van Dam et al., 2015).

Suppression of hypothalamic AMPK and ACC are associated with increased sympathetic nervous system activation, resulting in norepinephrine release and stimulation of β3-adrenergic receptors on brown adipocyte membrane (Martinez de Morentin et al., 2012; van Dam et al., 2015). Interestingly, AMPK activity in BAT has been reported to be associated with UCP1 activity. Representative AMPK activators AICAR, berberine (Zhang Z et al., 2014), gallic acid (Doan et al., 2015), metformin (Geerling et al., 2014), and resveratrol (Alberdi et al., 2013) have been demonstrated to contribute to BAT activation. Substances that can induce AMPK activity may induce various biological changes including regulation of energy metabolism in humans.

1.4.3 Representative AMPK activators

AICAR is mainly used to induce AMPK activation in *in vitro* and *in vivo* experimental paradigms. AICAR enters the cell by the adenosine transporter and is converted to 5-amino-4-imidazolecarboxamide ribotide by adenosine kinase. 5-amino-4-imidazolecarboxamide ribotide functions in a manner similar to AMP and activates AMPK (Sullivan et al., 1994; Corton et al., 1995). Liver kinase B1 (LKB1, a serine/threonine protein kinase), calcium/calmodulin-dependent protein kinase β (CaMKK β), and transforming growth factor β-activated kinase 1 are among the kinases that phosphorylate AMPK α subunit at Thr172 (Kim J et al., 2016). Statins such as metformin activate AMPK through serine 428 phosphorylation of LKB1. LKB1 was reported to bind the pseudokinase STRAD and the scaffolding protein MO25, which induce LKB1 (Zeqiraj et al., 2009). Additionally, LKB1 has been

shown to enhance the attachment of AMP to the AMPK γ subunit (Sakamoto et al., 2004). Conversely, CaMKK β is activated by Ca^{2+} to activate AMPK, and this signaling pathway appears to be independent of changes in intracellular AMP/ATP levels and plays an important role in neurons, vascular endothelial cells, and T lymphocytes. Transforming growth factor β-activated kinase 1is known to activate AMPK in tumor necrosis factor-mediated apoptosis (Momcilovic et al., 2006). Hormones and/or cytokines such as leptin, adiponectin, ghrelin, and cannabinoids, which regulate energy balance, can alter AMPK activity (Lim et al., 2010). Leptin, activates AMPK in skeletal muscle through hypothalamo-sympathetic axis (Minokoshi et al., 2002). However, leptin does not increase AMPK activity in diet-induced obese rats (Lee Y et al., 2004). Adiponectin activates AMPK in liver and muscle, leading to stimulation of glucose uptake and fatty acid oxidation (Yamauchi et al., 2002). Ghrelin and cannabinoids have been reported to stimulate hypothalamus and heart AMPK activity, while suppressed adipose tissue and liver AMPK activity (Kola et al., 2005; Kola et al., 2008).

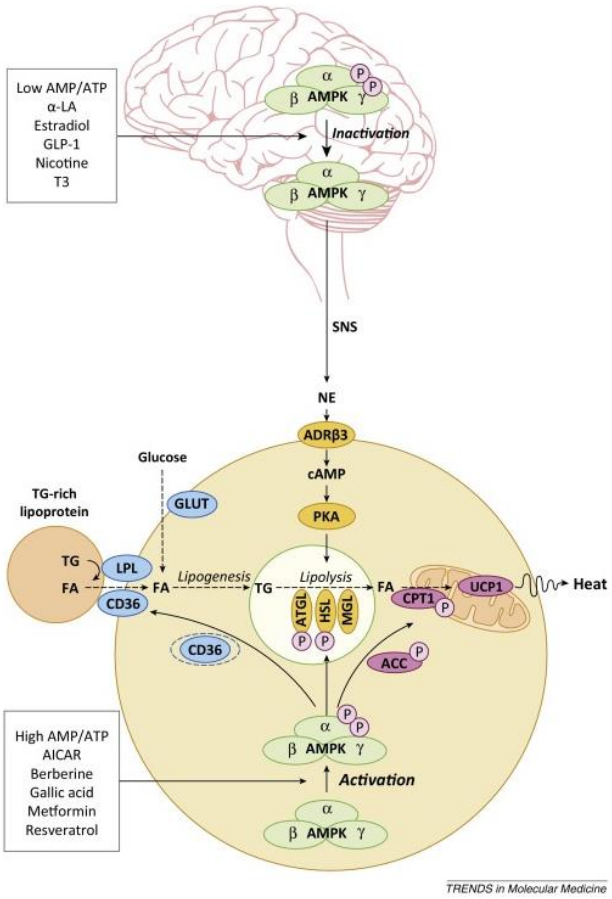

Figure 4. AMPK activity in the brain and in brown adipose tissue regulates thermogenesis (van Dam et al., 2015).

1. 5 *Saururus chinensis*

Saururus chinensis (*S. chinensis*) is a perennial herbaceous plant of the *Saururaceae* family and is referred to as Chinese lizard's tail or, in Korea, Sam-Baek-cho. *S. chinensis* is naturally grown or cultivated in China, India, Japan, Philippines, Vietnam, and Korea. It grows as a penumbra in moist places such as lowland wetlands and ponds. The aerial part of *S. chinensis* has been traditionally used to treat inflammatory diseases such as edema, gonorrhea, and asthma (Lee A Y et al., 2015), and findings from numerous studies provide support its anti-inflammatory effects (Lee E et al., 2006; Yoo et al., 2008; Quan et al., 2010). In addition, *S. chinensis* has been reported to function as an anti-oxidant (Cho et al., 2005; Yu et al., 2008; Kim B W et al., 2014), anti-tumor agent (Kim H Y et al., 2011; Jeong et al., 2015), hepatoprotectant (Wang L et al., 2009; Kwon et al., 2014), anti-fibrotic (Wang L et al., 2009), anti-hypertensive, vasorelaxant, and inotropic (Ryu et al., 2008), in addition to its inhibitory effect in atopic dermatitis (Choi M S et al., 2008) and lipid-lowering action (Yun et al., 2007; Yu et al., 2008). *S. chinensis* has several active ingredients such as lignans, alkaloids, diterpenes, flavonoids, tannins, steroids, and lipids (Kwon et al., 2014). Separation and structure identification of various unknown components of *S. chinensis* are currently under way, and its pharmacological effects have been reported in several studies (Li N et al., 2015; Li C et al., 2017). Sauchinone is a representative lignin isolated from *S. chinensis* and has been reported to protect liver against several types of liver injury through activate AMPK pathway (Kim et al., 2009; Kim et al., 2010) and inhibit proliferation of human hepatocellular carcinoma by regulation of AMPK-mTOR pathway (Kim et al., 2017)

2. Purpose of this study

Many anti-obesity drug have been developed to address the public health significance of obesity and high demand for its treatment. Current Food and Drug Administration-approved anti-obesity drugs include the lipid absorption inhibitor orlistat and the appetite suppressants phentermine, diethylpropion, and mazindol (Daneschvar et al., 2016). However, there are no drugs that are safe for long-term use without restrictions, which is a major concern as obesity is a chronic disease that requires long-term treatment and safety is essential. Anti-obesity treatments using natural products have been developed to fulfill the demand for safe and effective therapeutic agents. Unlike therapeutics with single ingredients, natural products exert anti-obesity effects through various mechanisms. Green tea, a natural product with a typical anti-obesity effect, has multiple anti-obesity effects such as reduction of appetite and lipogenesis and induction of lipolytic activity and energy expenditure (Thielecke et al., 2009). Similarly, *Hibiscus sabdariffa* has various effects as an anti-obesity agent, including reduction in plasma cholesterol and triglyceride levels, inhibition of gastric and pancreatic lipases, stimulation of thermogenesis, and inhibition of FAS (Herranz-Lopez et al., 2017). Similarly, *Garcinia cambogia* extract has multiple anti-obesity effects such as suppressed differentiation of adipocytes and reduction of fatty acid synthesis and appetite (Chuah et al., 2013).

Activation of the AMPK pathway in *in vivo* and *in vitro* obesity models has been shown to inhibit enzymes involved in lipid synthesis and to activate fatty acid

oxidation and thermogenesis. In particular, increasing energy consumption through energy burning in BAT and through browning in WAT are attracting attention as new targets for obesity treatment. Studies have shown that factors that induce UCP1 and other thermogenic factors have a significant effect on improving obesity. AMPK activation is associated with BAT heat generation, and many studies have been carried out on substances that affect BAT heat generation by activating the AMPK mechanism. *S. chinensis*, which has been traditionally used for the treatment of inflammatory conditions in East Asia, was recently reported to have anti-obesity effects. Although some of the *S. chinensis* components were reported to activate the AMPK pathway, the mechanisms underlying the anti-obesity effect have not been sufficiently elucidated, and there has been no study of heat production. The purpose of this study was to investigate the anti-obesity effect of *S. chinensis* in high fat diet-induced obese mice and to study the molecular mechanisms underlying the improvement of brown adipocyte functions by *S. chinensis* using IBA and 3T3-L1 and suppressed lipogenesis by *S. chinensis* using 3T3-L1 cells. Verification of *S. chinensis*-mediated anti-obesity effects through heat generation will contribute to the development of a new natural anti-obesity therapeutic agent.

Materials and Methods

1. Reagents and Antibodies

Dexamethasone, 3-isobutyl-1-methylxanthine (IBMX), 4% neutralized formalin solution, insulin, 3, 3',5-Triiodo-L-thyronine (T3), indomethacin, and Oil Red O were purchased from Sigma Chemical (St. Louis, MO, USA). Bovine serum, fetal bovine serum (FBS), goat serum, and 100 U/mL penicillin/10 ug/mL streptomycin (P/S) were purchased from Gibco (Carlsbad, CA, USA). Dulbecco's modified Eagle's medium (DMEM) was obtained from Lonza (Walkersville, MD, USA). Anti-SCD-1, anti-PPARγ, anti-FAS, anti-ACC, phospho-ACC, anti-AMPK, and phospho-AMPK were purchased from Cell Signaling Technology. (Boston, MA, USA). Anti-UCP1 and anti-PGC1α antibody were purchase from abcam. Anti-β-actin antibody and AMPKα1/2 siRNA (siAMPK) were purchased from Santa Cruz Biotechnology (Bergheimer, Heidelberg, Germany), and anti-β-tubulin antibody was purchased from Applied Biological Materials (Richmond, Canada). The anti-SREBP1 antibody was obtained from BD Biosciences (San Jose, CA, USA). Secondary antibodies for immunoblotting, and enhanced chemiluminescence reagents were purchased from Thermo Scientific (Rockford, IL, USA). Polyvinylidene fluoride membranes and radioimmunoprecipitation buffer were purchased from Millipore (Darmstadt, Germany). Phosphatase and protease inhibitor cocktails were purchased from Roche (Basel, Switzerland).

2. Ethanol Extraction of *S. chinensis*

S. chinensis was purchased from Youngcheon Hyundai Oriental Herbal Market (Youngcheon, South Korea). The purchased specimens were confirmed to be *S. chinensis* by Professor KiHwan Bae (Chung-nam National University, Korea), and they were stored at the herb bank of the KM-Application Center, Korea Institute of Oriental Medicine. Dried SC was crushed into small pieces by blender, 70% ethanol was added to a final concentration of 30 g/390 mL, and extraction was achieved in a shaking incubator at 40℃ for 24 h. *S. chinensis* ethanol extracts (SC) were filtered using 185-mm Whatman filter papers to remove suspended solids and concentrated using a rotary vacuum evaporator (Buchi, Japan). The concentrate was converted into powder form using a freeze dryer, with a final freeze-drying yield of 5.43%.

3. Identification of phytochemical constituents

The analyses were performed using a Dionex UltiMate 3000 system (Dionex Corp., Sunnyvale, CA, USA) equipped with Thermo Q-Exactive (Thermo Fisher Scientific, Bremen, Germany). The separation was performed on a Waters Acquity UPLC BEH C18 analytical column (2.1×100 mm, 1.7 μm), and mobile phase consisted of 0.1% formic acid in water (A, v/v) and acetonitrile (B). Gradient elution was programed as follows: 3.0% B, 0.0–1.0 min; 3.0–15.0% B, 1.0–2.0 min; 15.0–50.0% B, 2.0–13.0 min; 50–100% B, 13.0–20.0 min; 100–100% B, 20.0–23.0 min; 3–3% B, 23.0–27.5 min. The flow rate was 0.25 mL/min. The operation conditions in the mass spectrometry analysis were set as follows: ionization mode,

negative and positive ion-switching mode; spray voltage, 3.8 kV; capillary temperature, 320℃; sheath gas pressure, 40 arbitrary units; auxiliary gas pressure, 10 arbitrary units; ion scans, 100–1,500 m/z; resolution of MS scans, 70,000. Samples were prepared in methanol and filtered through a 0.22-μm filter membrane before injecting 3 μL of aliquots to LC-MS analysis.

4. Cell culture

3T3-L1 cells were purchased from the American Type Culture Collection (Manassas, VA, USA) and were cultured according to the supplier's recommendations. Briefly, 3T3-L1 cells were maintained in DMEM containing 10% BS and 1% P/S at 37℃ in a 5% CO_2 incubator. Two days after reaching full confluence, differentiation was induced in a differentiation medium (DMI) comprising DMEM supplemented with 10% FBS, 1% P/S, 1 μM dexamethasone, 0.5 mM IBMX, and 1 μg/mL insulin. After 2 days, the medium was replaced with DMEM supplemented with 10% FBS, 1% P/S, and 1 μg/mL insulin, which was later replaced with DMEM supplemented with 10% FBS and 1% P/S every other day until end of experiment. Drug treatment times were different for each experiment. Drugs were added before differentiation in experiments assessing inhibition of adipocyte differentiation and after differentiation for experiments assessing browning. Immortalized brown adipocytes (IBA), which were obtained from Professor Shingo at UCSF Diabetes Center (Department of Cell and Tissue biology, University of California, San Francisco, USA), were maintained in DMEM containing 10% FBS and 1% PS at 37℃ in a 5% CO_2 incubator. IBA cells

differentiated using 10 dexamethasone, IBMX, T3, indomethacin, and insulin were compared to those maintained in DMEM supplemented with 10% FBS, and 1% P/S. After 2 days, the medium was replaced with DMEM supplemented with 10% FBS, 1% P/S, insulin, and T3. After differentiation, IBA cells were treated with SC for 1 or 24 h.

siAMPK transfection was performed using Lipofectamine® RNAiMAX from Thermo Fisher, according to the manufacturer's instructions, and 10 nM siAMPK was added to culture medium for 24 h. The efficacy of siAMPK transfection was determined by assessment of AMPK protein expression by immunoblotting.

5. Animal experiments

The animal study was approved by the institutional animal care and use committee at the Korean Institute of Oriental Medicine (approval no, D-17-005), and all animal studies were performed according to the guidelines of the animal care and use committee at the Korean Institute of Oriental Medicine. Seven-week-old male C57BL/6J mice were purchased from Central Lab. Animal Inc. (Seoul, Korea) and housed in an environmentally controlled room with a temperature of 20℃–24℃ and a humidity of 40%–60% achieved with central air conditioning. All animals were maintained at a 12 h light/12 h dark cycle, and water was provided *ad libitum*. After a 1-week adaptation period, mice were randomly divided into five groups according to body weight: (1) low-fat-diet (LFD)-fed mice (LFD-vehicle); (2) LFD-fed mice treated with 100 mg/kg body weight SC (LFD-SC-100); (3) 60% kcal fat-diet (HFD)-fed mice (HFD-vehicle); (4) HFD-fed mice treated with 50

mg/kg body weight SC per day (HFD-SC-50); and (5) HFD-fed mice treated with 100 mg/kg body weight SC per day (HFD-SC-100). The HFD (D12492) was purchased from Research Diet (New Brunswick, NJ, USA) and LFD (5053) purchased from TestDiet (Brentwood, Mo, USA). SC powder was re-suspended in sterile saline and administered orally six times per week during the high-fat-feeding period, with an oral administration volume of 5 mL/kg body weight, and LFD-vehicle and HFD-vehicle groups received same saline volumes orally. After 14 weeks of the experimental period, mice were anesthetized with 2.5% isoflurane (Hana Pham, Gyeonggi-do, Korea) in oxygen, blood was collected, and organs were harvested after perfusion. All organs were rinsed with saline solution, immediately frozen in liquid nitrogen, and stored at −80℃.

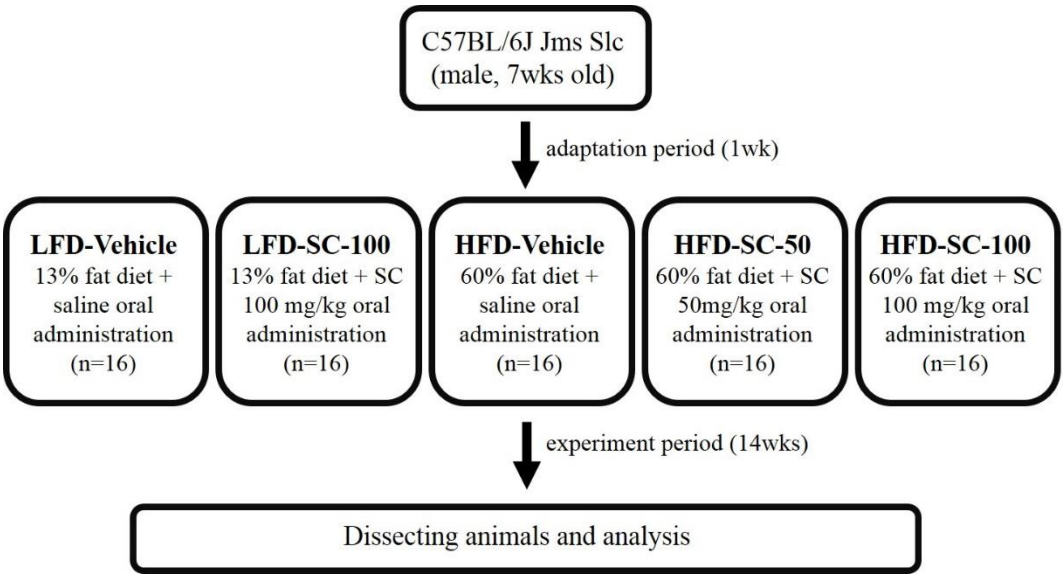

Figure 5. Experimental design of HFD-induced obesity mice.

6. Glucose tolerance test

Glucose tolerance test was performed at 10 weeks after obesity induction. All mice were fasted overnight before the test. A glucose solution (1 g/kg body weight) was intraperitoneally injected, and a glucometer (Accu-chek, Roche, Mannheim, Germany) was used for tail blood glucose measurements at 0, 15, 30, 60, and 120 min after glucose injection.

7. Assessment of metabolic rate, physical activity, and fat mass

Metabolic rate and physical activity were measured using an indirect calorimetry (Columbus Instruments Comprehensive Lab Animal Monitoring System), according to the manufacturer's instructions. O_2 analyzers were calibrated with highly purified gas standards. Mice were placed in individual chambers at 25℃ under a 12-h light/12-h dark cycle for 72 h. Water and food were supplied *ad libitum*. VO_2, activity, and heat production were automatically calculated. Fat mass was measured using Bruker's minispec LF 50 Body Composition Analyzer (Brunker, Germany), according to the manufacturer's instructions.

8. Thermal images and micro-positron emission tomography/computed tomography (Micro-PET/CT)

The thermal images were collected using an infrared thermographic camera (Therma T620, FLIR, Canada). Micro-PET/CT imaging was performed by a Triumph II PET/CT system (LabPET8, Gamma Medica-Ideas) at the Graduate

School of Medicine, Kyungpook National University. Mice were injected with 7.4 MBq ^{18}F-fluorodeoxyglucose (FDG) via tail vein before CT scanning. The PET imaging system had the following specifications: ring diameter, 162 mm; field of view (FOV), 60 mm; crystals, 3072; spatial resolution, 1.35-mm full-width half-maximum (FWHM) FOV; and noise-equivalent counts, 37 kcps at 245 MBq (250–650 keV). CT scanning was achieved with an X-ray detector (fly acquisition, 512 projections; binning setting, 2 × 2; frame number, 1; X-ray tube voltage, 75 kVp; focal spot size, 50 μm; magnification factor, 1.5; matrix size, 512) immediately after PET imaging. PET images were reconstructed by 3D-ordered subsets expectation-maximization iterative image reconstruction, and CT images were reconstructed using filtered back-projections. All mice were anesthetized with 1–2% isoflurane during imaging. Functional PET images were coregistered with anatomical CT images using the 3D image visualization and analysis software VIVID (Gamma Medica-Ideas). The uptake (% ID/cc) for volumes of interest from each image was determined by manually selecting BAT in coregistered CT images using the PMOD 3.5 software (PMOD Technologies).

9. Serum chemistry

Blood samples were collected from abdominal vena cava to measure the following parameters using a biochemical analyzer XL-200 (ERBA Mannheim, Germany): aspartate aminotransferase (AST), alanine aminotransferase (ALT), lactate dehydrogenase (LDH), low-density lipoprotein cholesterol (LDL-C), high-density lipoprotein cholesterol (HDL-C), triglyceride, glucose, urea, and creatinine. Serum

FFA levels were determined by a colorimetric method using an FFA quantification kit from Biovision (Korea). Insulin, leptin, and adiponectin levels were measured using mouse adiponectin/Acrp30 immunoassay kit (R&D Systems, Minneapolis, MN, USA), Morinaga mouse/Rat leptin ELISA kit (MIoBS, Japan), and Morinaga ultrasensitive mouse/rat insulin ELISA kit (MIoBS, Japan), respectively, according the manufacturers' protocols.

10. Quantitative real-time reverse transcription-polymerase chain reaction

For quantitative real-time reverse transcription-polymerase chain reaction (RT-PCR), total RNA was extracted from organs using TRIzol^{TM} reagent (QIAGEN, Germany), according to the manufacturer's protocol, and extracted RNA was analyzed for purity and concentration using a Nano-Drop spectrophotometer (Thermo Scientific, Waltham, MA, USA). cDNA was synthesized from 1 ug of total RNA using cDNA synthesis kit for RT-PCR (Thermo Scientific, Waltham, MA, USA), according to the manufacturer's protocol, and analyzed on a CFX96 real-time system (BioRad Laboratories, USA). Primer sequences for qPCR are listed in Table 1. Cycle threshold (CT) data were normalized using 36B4 mRNA, and relative mRNA expression levels were calculated using the $2^{(-\Delta\Delta CT)}$ method.

Table 1. Primer sequences for RT PCR.

Gene	Sequences(5'→3') of the Real-time PCR primers
C/EBPα	sense – GCGCAAGAGCCGAGATAAAG
	antisense - CGGTCATTGTCACTGGTCAACT
PPARγ	sense – CACAAGAGCTGACCCAATGGT
	antisense - GATCGCACTTTGGTATTCTTGGA
SREBP-1	sense – CCCTACCGGTCTTCTATCAATGA
	antisense - GCAGATTTATTCAGCTTTGCTTCA
FAS	sense – ACCTGGTAGACCACTGCATTGAC
	antisense - CCTGATGAAACGACACATTCTCA
ACC	sense - CGCTCAGGTCACCAAAAAGAAT
	antisense - GGGTCCCGGCCACATAA
SCD-1	sense - CTGCCCCTGCGGATCTT
	antisense - GCCCATTCGTACACGTCATTCT
Adiponectin	sense-CTCCACCCAAGGGAACTTGT
	antisense-GGACCAAGAAGACCTGCATC
Cidea	sense-GCCGTGTTAAGGAATCTGCTG
	antisense-TGCTCTTCTGTATCGCCCAGT
Dio2	sense-TTGGGGTAGGGAATGTTGGC
	antisense-TCCGTTTCCTCTTTCCGGTG
NRF1	sense-CAGCAACCCTGATGGCACCGTGTC
	antisense-GGCCTCTGATGCTTGCGTCGTCTG

PGC1α	sense-GCCCAGGTACGACAGCTATG antisense-ACGGCGCTCTTCAATTGCTT
PRDM16	sense-AGCCCTCGCCCACAACTTGC antisense-TGACCCCCGGCTTCCGTTCA
TFAM	sense-AGTTCCCACGCTGGTAGTGT antisense-GCGCACATCTCGACCC
UCP1	sense-CTTTGCCTCACTCAGGATTGG antisense-CTTTGCCTCACTCAGGATTGG
GLUT1	sense-ATACCTCTACATCATCCGGA antisense-AGCTAGTGCGTCAGACACAT
GLUT4	sense-CCGGATTCCATCCCACAAG antisense-TCATGCCACCCACAGAGAAG
PPARα	sense-GAACAAAGACGGGATGCTC antisense-ACAGAACGGCTTCCTCAGGTT
ATGL	sense-CCTCAGGACAGCTCCACCA antisense-GATTGCGAAGGTTGAACTGGAT
HSL	sense-CCGAGATGTCACAGTCAATGGA antisense-CCAGGCCGCAGAAAAAAG
36B4	sense-ACCTCCTTCTTCCAGGCTTT antisense-CTCCAGTCTTTATCAGCTGC

11. Western immunoblotting

For protein expression analysis, samples were homogenized in radioimmuno-precipitation buffer containing phosphatase and protease inhibitor cocktails. After centrifugation, supernatants were collected, and protein concentrations were determined using the BCA protein assay kit (Thermo Scientific, Rockford, IL, USA). Protein extracts were separated using sodium dodecyl sulfate-polyacrylamide gel electrophoresis and transferred to polyvinylidene fluoride membranes, which were then immunoblotted with specific primary antibodies for indicated proteins and detected by appropriate horseradish peroxidase-conjugated secondary antibodies. Chemiluminescence signals were detected using the ChemiDoc Touch imaging system (BioRad Laboratories, USA), and band intensities were quantified using ImageJ software (National Institutes of Health, USA).

12. Histological analysis

Liver, WAT, and BAT specimens were fixed with 4% paraformaldehyde immediately after dissection, dehydrated in a graded ethanol series (70–100%), and embedded in paraffin. Paraffin blocks were sectioned at 4-μm-thick slices, and paraffin sections were deparaffinized, rehydrated, and stained by hematoxylin/eosin for immune-histochemistry. Briefly, antigen retrieval was achieved with a citrate-based buffer, and sections were incubated with an anti-UCP1 antibody at 4℃ overnight. Next, sections were incubated with a biotinylated anti-rabbit IgG antibody and Vectastain ABS reagent (Vector Laboratories, CA,

USA) for 3 h. Next, the sections were incubated with DAB alkaline phosphatase substrate (SK-4100, Vector Laboratories) for visualization of the brown staining. Sections were visualized using an Olympus digital camera system, and images were captured at 400× magnification.

13. Immunofluorescence

Following treatment for 24 h with or without SC, IBA cells were fixed in 10% neutralized formalin solution and then washed with phosphate buffered saline containing TritonX-100. Subsequently, IBA cells were incubated in 5% goat serum for 1 h, followed by overnight treatments with primary antibodies at 4℃. IBA cells were then incubated with Alexa-Fluor-labeled secondary antibody for 3 h at room temperature and were finally mounted with 4',6-diamidino-2-phenylindole (dapi). Immunofluorescence was detected using a Olympus fluorescence microscope (Olympus, Tokyo, Japan).

14. Statistical analysis

Values were expressed as means ± standard error. Statistical significance of groups were analyzed using one-way analysis of variance, differences were determined using Dunnett’s test. Comparisons between the two groups were analyzed by t-test. All analyses were performed using Graphpad Prism software.

Results

1. SC inhibits lipogenesis in 3T3-L1 cells

To elucidate the effects of SC on lipogenesis, 3T3-L1 cells were differentiated with or without SC for 8 days. As shown in Figure 6, mature lipid droplets were observed visually in differentiated adipocytes with no SC treatment (control). However, lipid droplet accumulation was inhibited in differentiated cells treated with SC. Additionally, quantitative measurement of triglyceride levels by dissolving Oil Red O-stained lipid droplets in isopropanol revealed that the amount of triglycerides in the SC-treated cells was 80% lower than those in the controls, and the effect was significant even at an SC concentration of 1 ug/ml. Differentiated 3T3-L1 cells exhibited increased expression of lipogenesis-associated genes and proteins, whereas the SC treatment inhibited several adipogenic factors such as FAS, SREPB1, ACC, SCD-1, CCAAT/enhancer-binding protein (C/EBP)α, and PPARγ. These analyses revealed that the levels of all adipogenic factors were significantly decreased by SC treatment, compared to the control, and these results were corroborated by the changes in triglyceride levels (Figure 7).

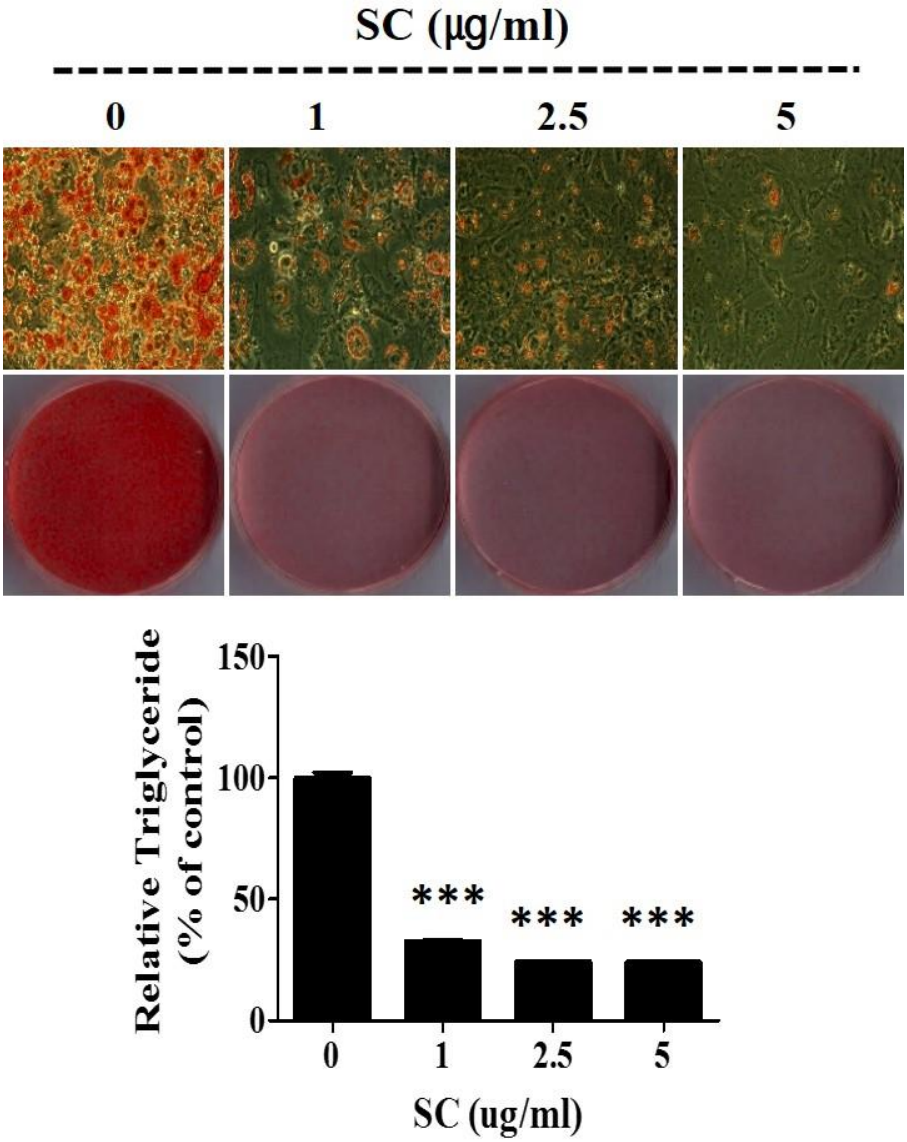

Figure 6. SC inhibits lipid accumulation during adipocyte differentiation.

3T3-L1 cells undergo differentiation induced by DMI with or without SC. Lipid accumulation was examined by Oil Red O staining. Oil Red O-stained cells were photographed and red-stained lipids were extracted with isopropyl alcohol, and the absorbance at 520 nm was measured. The data were presented as the means ± SEM. * $p < 0.05$, ** $p < 0.01$, ***$p < 0.001$, compared to DMI induced without SC treatment.

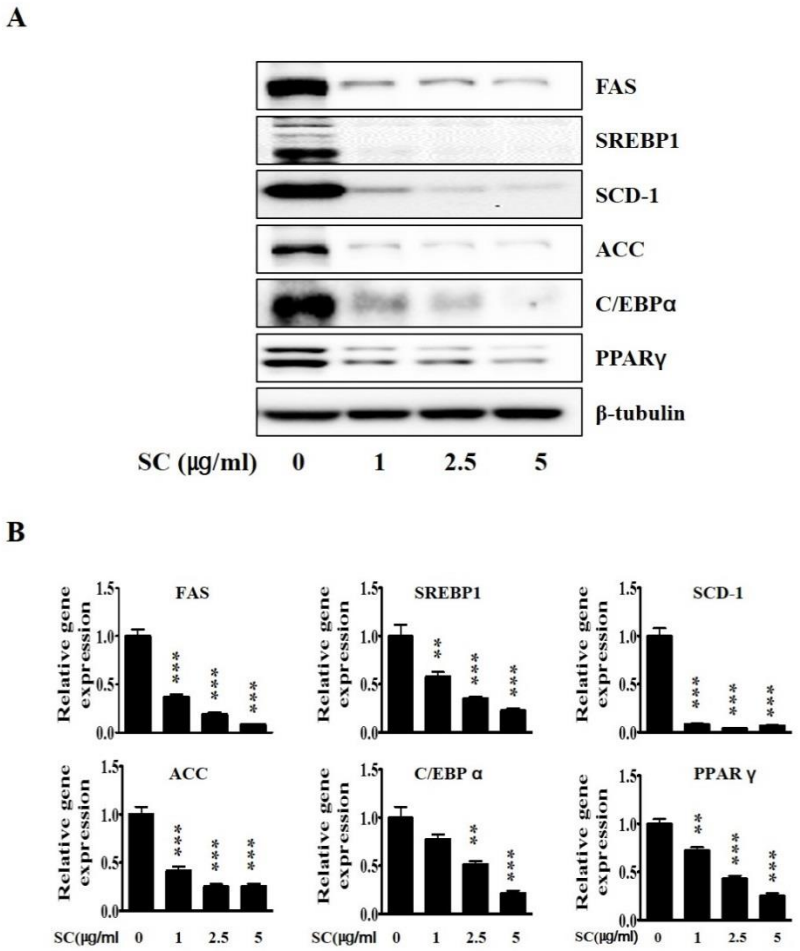

Figure 7. SC inhibits DMI-induced protein and gene expression related to adipogenesis.

3T3-L1 cells were differentiated for 8 days with or without SC. After 8 days of differentiation, mRNA and protein were extracted. The protein expression was examined by western blotting (A). The mRNA expression was examined by real-time PCR and the gene expression data were normalized to 36B4 and analyzed using the $2(^{-\Delta\Delta CT})$. The data were presented as the means ± SEM. *$p < 0.05$, **$p < 0.01$, ***$p < 0.001$, compared to DMI induced without SC treatment.

2. SC activates AMPK signaling

To investigate the mechanisms underlying anti-adipogenic effects of the SC, protein expression of the 3T3-L1 cells was assessed during the early stage of differentiation. Although SC treatment did not affect DMI-induced AKT phosphorylation, SC treatment increased LKB1, AMPK, and ACC phosphorylation at the early stage of differentiation. AMPK knockdown was achieved using siRNA in 3T3-L1 cells to determine whether AMPK pathway was necessary for the effects of the SC on adipogenesis. As shown in Figure 8, a decrease in SC-mediated changes in adipogenesis was observed in cells transfected with siAMPK. These results indicated that SC treatment activated the AMPK pathway in 3T3-L1 cells, which significantly inhibited adipogenesis.

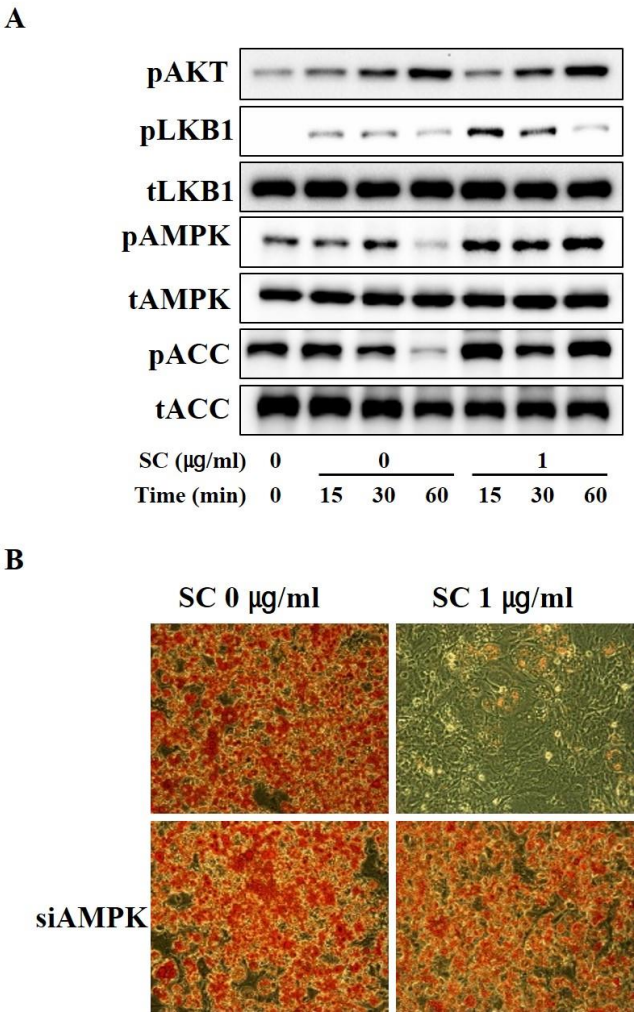

Figure 8. SC inhibit DMI-induced adipogenesis through AMPK activation in 3T3-L1 cells.

Fully confluent preadipocytes were differentiated via DMI with or without SC. The protein was extracted at 0, 15, 30, and 60 min of differentiation with or without SC. The protein expression was examined by western blotting (A). 3T3-L1 cells were transfected with AMPK siRNA for 24h and fully confluent preadipocytes were differentiated via DMI with or without SC. Lipid accumulation was examined by Oil Red O staining (B).

3. Effect of SC on body weight gain in mice with HFD-induced obesity

To investigate the inhibitory effect of SC on body gain, body weight was measured once a week in mice fed with HFD or LFD. As shown in Figure 9, a significant difference in body weight was observed between the two groups after 1 week of feeding ($p < 0.01$), and the difference in body weight increased over time ($p < 0.001$). At 2 weeks after the start of the experiment, the body weight was significantly lower in HFD mice treated with SC than in untreated HFD mice ($p < 0.05$); the gap in body weight between the two groups increased over time ($p < 0.001$). In addition, total body weight gain was higher in the HFD-vehicle group than in the LFD-vehicle group (24.24 ± 0.49 vs. 5.80 ± 0.32 g). However, the weight gain was significantly inhibited with the administration of SC, and the effect was dose-dependent (19.34 ± 0.72 and 11.47 ± 0.73 g weight gain in the HFD-SC-50 and HFD-SC-100 groups, respectively). However, in LFD mice, SC-100 administration did not cause weight loss. These results suggested that SC inhibited HFD-mediated weight gain in mice.

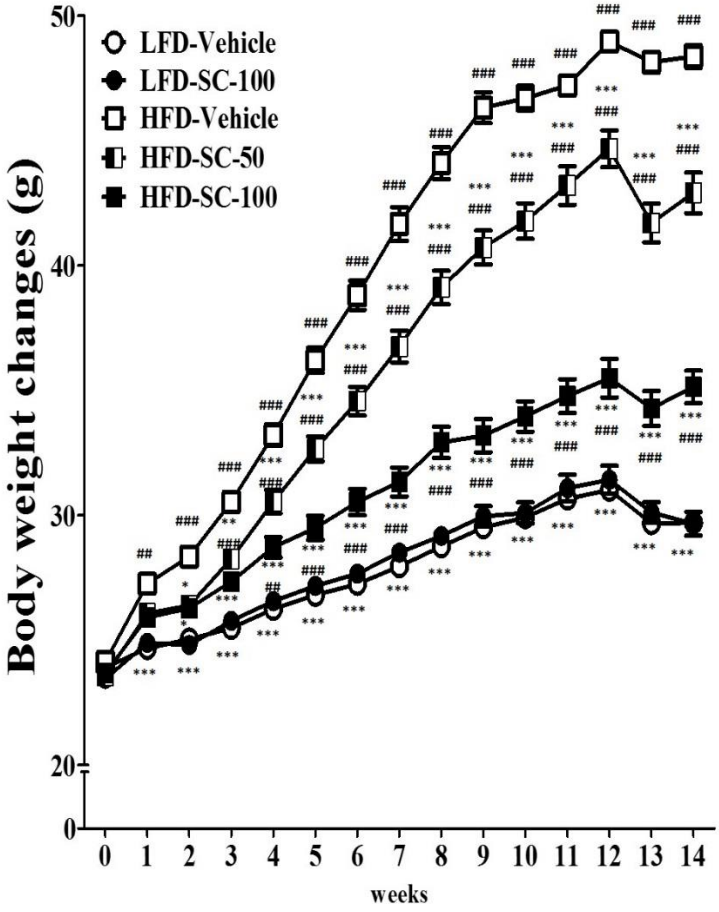

Figure 9. SC inhibited body weight gain in HFD-fed mice.

C57BL/6J mice were fed LFD and HFD for 14 weeks, and body weight was measured once a week during the experimental period. The data were presented as the means ± SEM. * $p < 0.05$, ** $p < 0.01$,*** $p < 0.001$, compared to HFD-Vehicle; # $p < 0.05$, ## $p < 0.05$, ### $p < 0.001$, compared to LFD-Vehicle; LFD, low-fat-diet; HFD, high-fat- diet; LFD-Vehicle, LFD fed mice treated with 0 mg/kg body weight SC (n=16); LFD-SC-100, LFD fed mice treated with 100 mg/kg body weight SC (n=16); HFD-Vehicle, HFD fed mice 0 mg/kg body weight SC (n=16); HFD-SC-50, HFD fed mice treated with 50 mg/kg body weight SC (n=16); HFD-SC-100, HFD fed mice treated with 100 mg/kg body weight SC (n=16).

4. Effect of SC on fat mass and size in mice with HFD-induced obesity

Changes in body fat mass and size in HFD mice and LFD mice are shown in Figure 10. There was an approximately 4.1-fold increase in the fat mass in the HFD-vehicle group compared with that in the LFD-vehicle group, and the fat mass per body weight was 20.15% in the LFD group and 51.94% in the HFD group. However, the increase in fat mass in the HFD-SC-50 and HFD-SC-100 groups were only 3.4-fold and 2.1-fold; in addition, the ratios of fat mass per body weight were 46.90% and 35.70% in the HFD-SC-50 and HFD-SC-100 groups, respectively. The adipocyte size was decreased by the administration of SC. Specifically, the mean adipocyte size decreased by 28% in the HFD-SC-100 group compared with that in the HFD group that received vehicle. Conversely, lean mass did not change significantly among the groups. As shown in Figure 8, the distribution of adipocyte size in the LFD group was observed only smaller than 5000 um^2. However, size of over 5000 um^2 existed in a large proportion in HFD groups. Approximately 15% of adipocyte in the HFD-vehicle group were found to have a size of more than 10,000 um^2, but in the HFD-SC-100 group, only 2% of adipocyte were found to have a size of more than 10,000 um^2 (Figure 11). There were no significant differences in adipocyte size and distribution between the LFD-vehicle and LFD-SC-100 groups.

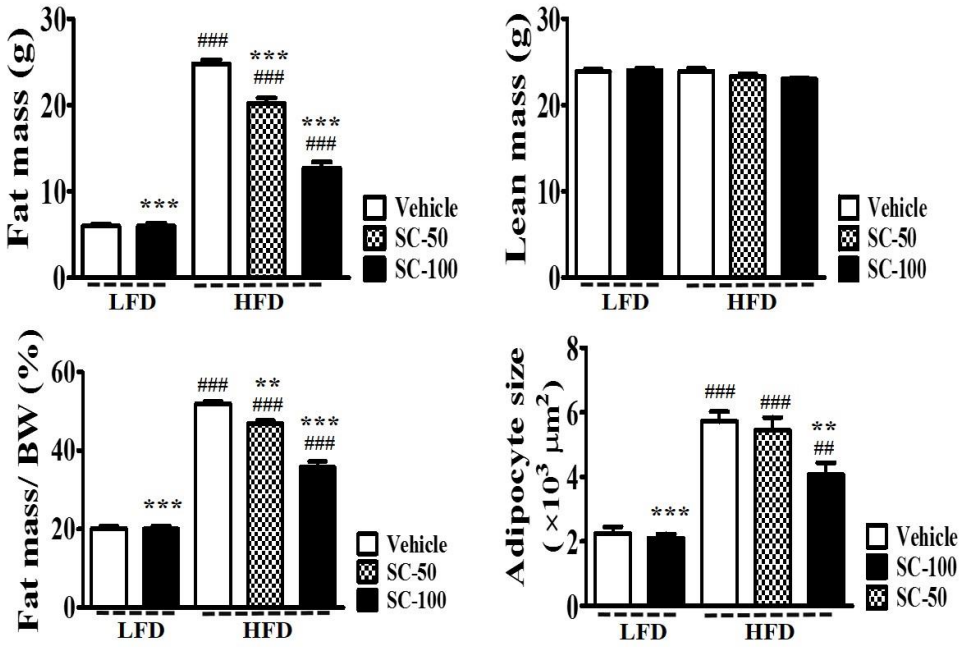

Figure 10. SC decreased fat mass and size in HFD-fed mice.

Fat mass and lean mass were measured by Bruker's minispec LF 50 Body Composition Analyzer. The paraffin sections of epididymal adipose tissue were stained with H&E, and then photographed to measure the size of adipocytes. The size of adipocytes was analyzed using the Adiposoft program. The data were presented as the means ± SEM. * $p < 0.05$, ** $p < 0.01$,*** $p < 0.001$, compared to HFD-Vehicle; # $p < 0.05$, ## $p < 0.05$, ### $p < 0.001$, compared to LFD-Vehicle. LFD, low-fat-diet–fed mice; HFD, high-fat-diet-fed mice; Vehicle- mice treated with 0 mg/kg body weight SC; SC-50, mice treated with 50 mg/kg body weight SC; SC-100, mice treated with 100 mg/kg body weight SC.

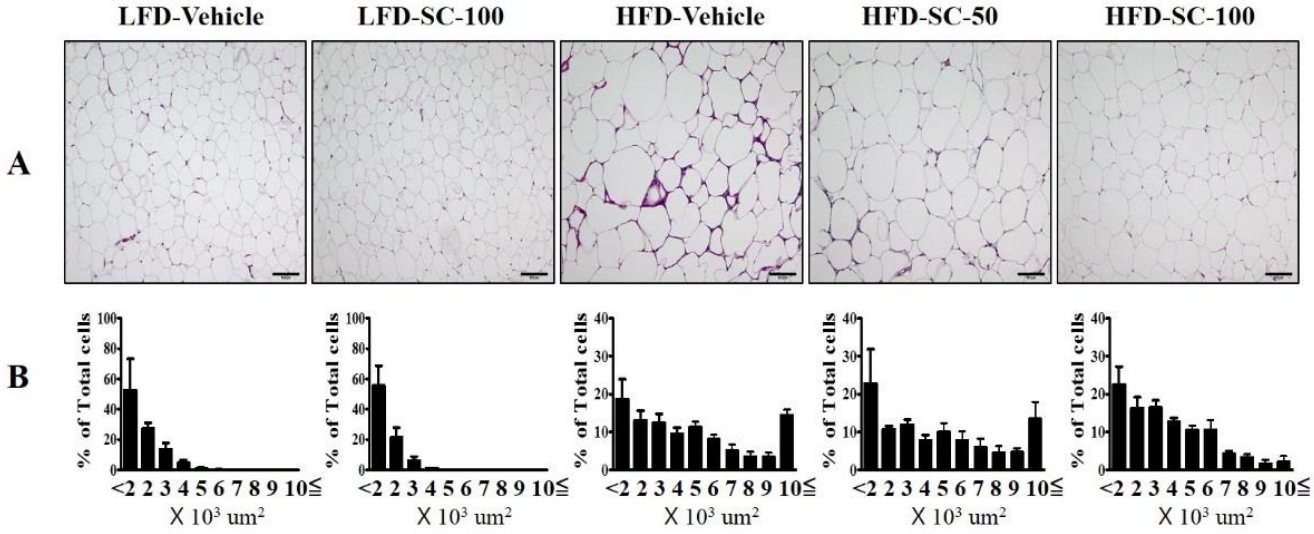

Figure 11. SC improved adipocyte size distribution in HFD-fed mice.

The paraffin sections of epididymal adipose tissue were stained with H&E, and then photographed (A). The size of adipocytes was analyzed using the adiposoft program (B). LFD, low fat diet; HFD, high fat diet; LFD-Vehicle, LFD fed mice; LFD-SC-100, LFD fed mice treated with 100 mg/kg body weight SC; HFD-Vehicle, HFD fed mice; HFD-SC-50, HFD fed mice treated with 50 mg/kg body weight SC;HFD-SC-100, HFD fed mice treated with 100 mg/kg body weight SC.

5. SC inhibits steatosis in HFD-fed mice

Feeding mice with HFD induces fat formation not only in adipose tissue but also in non-adipose tissues. Liver is the most frequently impacted tissue where these changes occur because of dietary factors, and steatosis is associated with obesity. As shown in Figure 12, the liver weight was approximately 1.8-fold higher in the HFD-vehicle group than in the group, and the difference was statistically significant ($p < 0.001$). However, in the LFD-vehicle group, the liver weight was significantly lower in the HFD-SC-100 group than in the HFD group, and there was no statistically significant difference between the HFD-SC-100 and the LFD groups. To determine if liver weight gain was because of fat accumulation, liver tissue specimens were stained with hematoxylin/eosin, which revealed the presence of fat accumulation in the HFD group and comparable changes between the HFD-SC-100 and the LFD groups (Figure 13). Serum AST and ALT levels, clinically important indicators of hepatotoxicity, were also higher in the HFD-vehicle group than the LFD-vehicle group (approximately 2.4-fold and 6.3-fold higher, respectively, $p < 0.001$). However, the serum AST and ALT levels, which were significantly lower in the HFD-SC groups than in the HFD-vehicle group, were comparable to those in the LFD-vehicle group. Of note, the administration of the SC did not lead to significant changes in the serum AST and ALT levels among the LFD groups, suggesting that SC administration alone was not associated with hepatotoxicity.

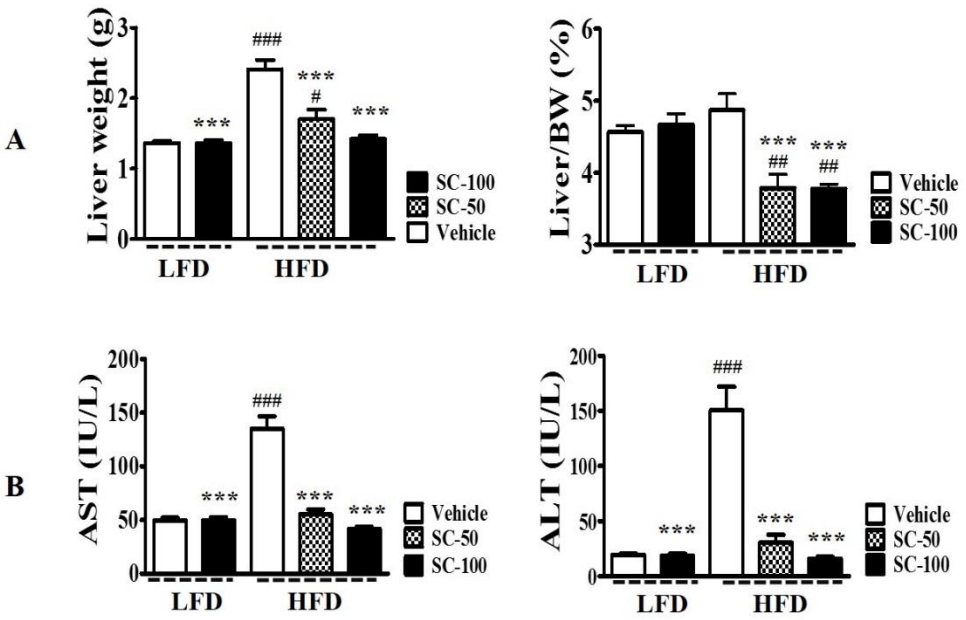

Figure 12. SC suppressed HFD-induced hepatic injury.

The liver weight were measured from mice at the end of study and weighed (A). The AST and ALT were measured with the serum of the autopsied animal (B). The data were presented as the means ± SEM. * $p < 0.05$, ** $p < 0.01$,*** $p < 0.001$, compared to HFD-Vehicle; # $p < 0.05$, ## $p < 0.05$, ### $p < 0.001$, compared to LFD-Vehicle (ANOVA with dunnett's test). BW, body weight (g); LFD, low fat diet; HFD, high fat diet; AST, aspartate aminotransferase; ALT, alanine aminotransferase; Vehicle, treated with 0 mg/kg body weight SC; SC-50, treated with 50 mg/kg body weight SC; SC-100, treated with 100 mg/kg body weight SC.

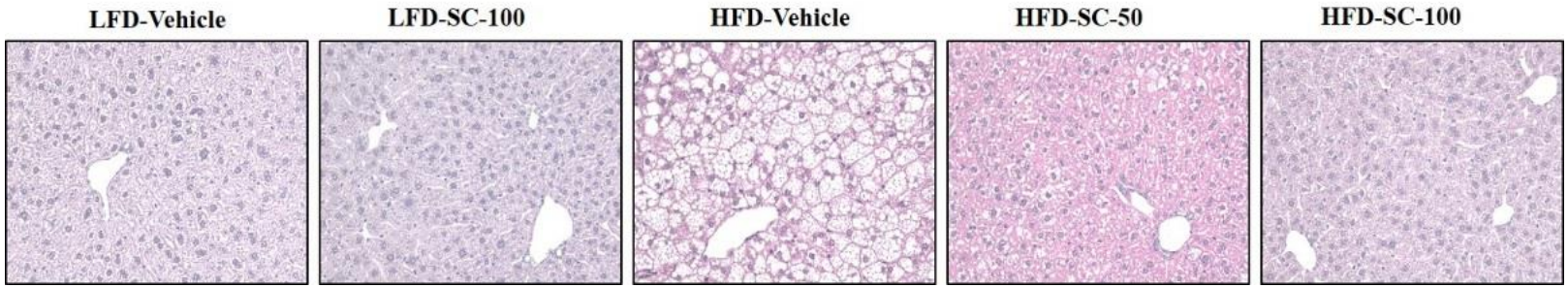

Figure 13. SC inhibited steatosis in HFD-fed mice.

The paraffin sections of liver tissue were stained with H&E, and then photographed. LFD, low fat diet; HFD, high fat diet; LFD-Vehicle, LFD fed mice treated with 0 mg/kg body weight SC; LFD-SC-100, LFD mice treated with 100 mg/kg body weight SC; HFD-Vehicle, HFD fed mice treated with 0 mg/kg body weight SC; HFD-SC-50, HFD fed mice treated with 50 mg/kg body weight SC;HFD-SC-100, HFD fed mice treated with 100 mg/kg body weight SC.

6. Effect of SC on serum chemistry

As shown in Table 2, LDH, a representative index of tissue damage, was significantly higher in the HFD-vehicle than in the LFD group; however, the LDH levels were significantly lower in all groups treated with the SC, which had a dose-dependent effect. Conversely, there were no significant differences in renal toxicity indices, BUN and creatinine, in any of the groups. Serum TC and LDL-C levels, which were significantly higher in the HFD-vehicle group than in the LFD-vehicle group, were significantly decreased by SC treatment. Although serum HDL-C levels were decreased in the HFD-SC-100 group, the HDL-C/TC ratios were not significantly different between the HFD-vehicle and HFD-SC groups. Blood glucose and serum insulin levels were also significantly higher in the HFD-vehicle group, which were significantly decreased with SC administration. Furthermore, the FFA levels were significantly decreased by SC administration in HDF mice, and the levels was similar to those observed in LFD groups.

Table 2. SC improved metabolic profiles in HFD-fed mice.

	LFD-Vehicle	LFD-SC-100	HFD-Vehcle	HFD-SC-50	HFD-SC-100
LDH (IU/L)	361.00 ± 52.27	251.50 ± 44.69**	578.00 ± 106.30#	111.50 ± 26.82***,#	99.00 ± 21.71***,#
Urea (mg/dl)	31.65 ± 1.52	27.90 ± 1.90	27.64 ± 1.32	28.15 ± 3.40	26.70 ± 2.72
Creatinine (mg/dl)	0.4 ± 0.0	0.4 ± 0.0	0.4 ± 0.0	0.4 ± 0.0	0.4 ± 0.0
Triglyceride (mg/dl)	69.00 ± 4.77	75.00 ± 4.12	85.00 ± 4.58	84.00 ± 4.90	82.50 ± 3.62
TC (mg/dl)	92.30 ± 3.88	94.20 ± 4.66***	208.80 ± 9.79###	165.05 ± 7.03***,###	153.80 ± 7.89***,###
HDL-C (mg/dl)	70.65 ± 3.54	71.45 ± 3.86***	165.10 ± 7.34###	132.50 ± 6.67**,###	124.90 ± 6.98***,###
LDL-C (mg/dl)	7.85 ± 0.36	7.75 ± 0.30***	26.75 ± 2.84###	15.80 ± 0.89***,##	12.40 ± 0.88***
TC/HDL-C ratio	1.31 ± 0.02	1.32 ± 0.01	1.27 ± 0.01	1.25 ± 0.01#	1.24 ± 0.01##
Glucose (mg/dl)	109.75 ± 4.59	101.88 ± 2.65**	167.25 ± 9.91###	145.75 ± 7.88##	128.50 ± 7.98***
Insulin (ng/ml)	0.34 ± 0.10	0.36 ± 0.11***	2.73 ± 0.75###	0.95 ± 0.29**	0.26 ± 0.03***
FFA (uM)	524.60 ± 44.47	464.80 ± 39.91**	637.40 ± 45.92	470.80 ± 20.40*	445.20 ± 24.61**

The data were presented as the means ± SEM. * $p < 0.05$, ** $p < 0.01$, *** $p < 0.001$, compared to HFD-Vehicle; # $p < 0.05$, ## $p < 0.05$, ### $p < 0.001$, compared to LFD-Vehicle (ANOVA with dunnett's test). LDH, lactate dehydrogenase; TC, total cholesterol, LDL-C, low-density lipoprotein cholesterol; HDL-C, high-density lipoprotein cholesterol; FFA, free fatty acid.

7. Effect of SC on serum adipokine levels

Adipokines such as adiponectin and leptin play an important role in insulin sensitivity and steatosis. In this study, the serum leptin levels were markedly increased in the HFD-vehicle group ($p<0.001$) compared with those in the LFD-vehicle group; however, the serum leptin levels were markedly decreased in a dose-dependent manner in the groups that received SC treatment. However, adiponectin levels were not significantly different between the treatment groups. TNF-α is the representative pro-inflammatory cytokine, resulting in the release of other inflammatory cytokines such as IL-1β and IL-6 (Chen et al., 2002) and obese humans exhibit increased circulating levels of TNF-a (Hotamisligil et al., 1995; Kern et al., 1995; Kern et al., 2001). TNF-a level was lower in HFD-SC-100 group compared with HFD-Vehicle, but the difference was not significantly (Figure 14).

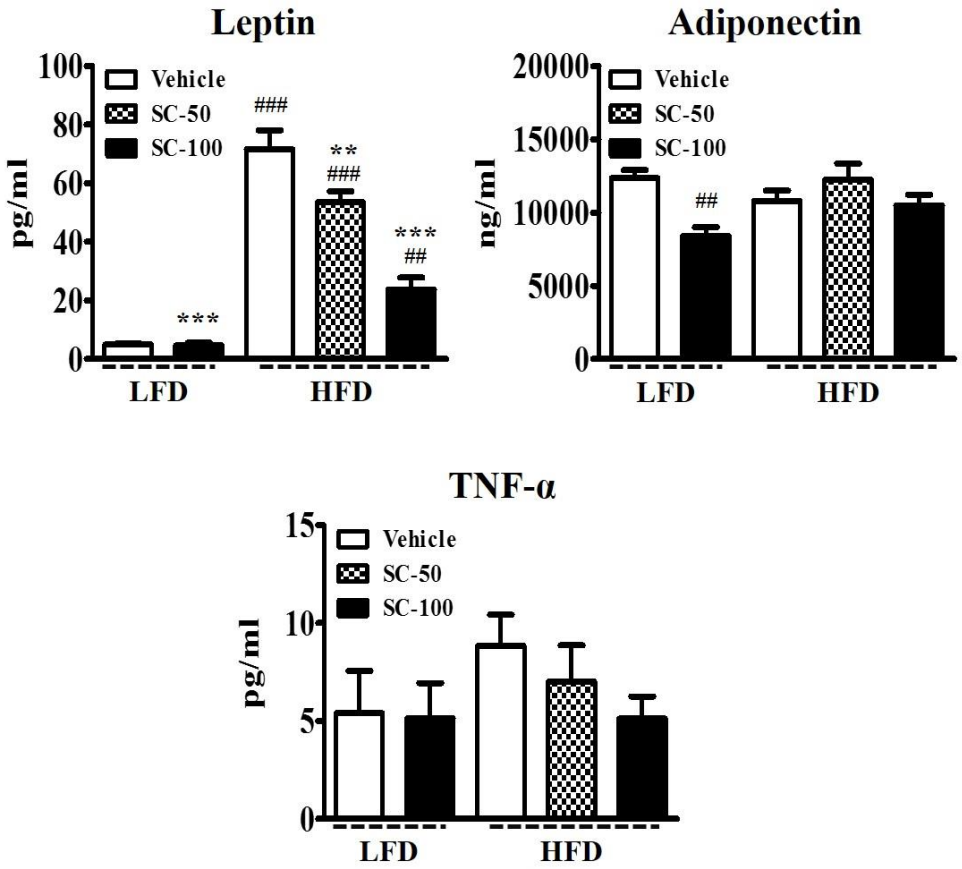

Figure 14. SC improved serum adipokine level.

The leptin, adiponectin, and TNF-α were measured with the serum of the autopsied animal. The data were presented as the means ± SEM. * $p < 0.05$, ** $p < 0.01$,*** $p < 0.001$, compared to HFD-Vehicle; # $p < 0.05$, ## $p < 0.05$, ### $p < 0.001$, compared to LFD-Vehicle (ANOVA with dunnett's test). LFD, low fat diet; HFD, high fat diet; Vehicle, treated with 0 mg/kg body weight SC; SC-50, treated with 50 mg/kg body weight SC; SC-100, treated with 100 mg/kg body weight SC.

8. Effect of SC on glucose tolerance

GTT was performed to examine the effect of SC administration on glucose tolerance. As shown in Figure 15, the HFD-vehicle group showed a significant increase in blood glucose levels in response to intraperitoneal glucose injection compared with the LFD-vehicle group. Blood glucose levels at 15 and 30 min after glucose injection were significantly decreased in the groups that were administered SC. The area under the curve (AUC) was significantly increased by HFD (31196 vs. 22823 with LFD). In contrast, AUC was significantly decreased by SC administration (29,168 and 27,470 with 50 and 100 mg/kg SC administration, respectively) (Figure 16).

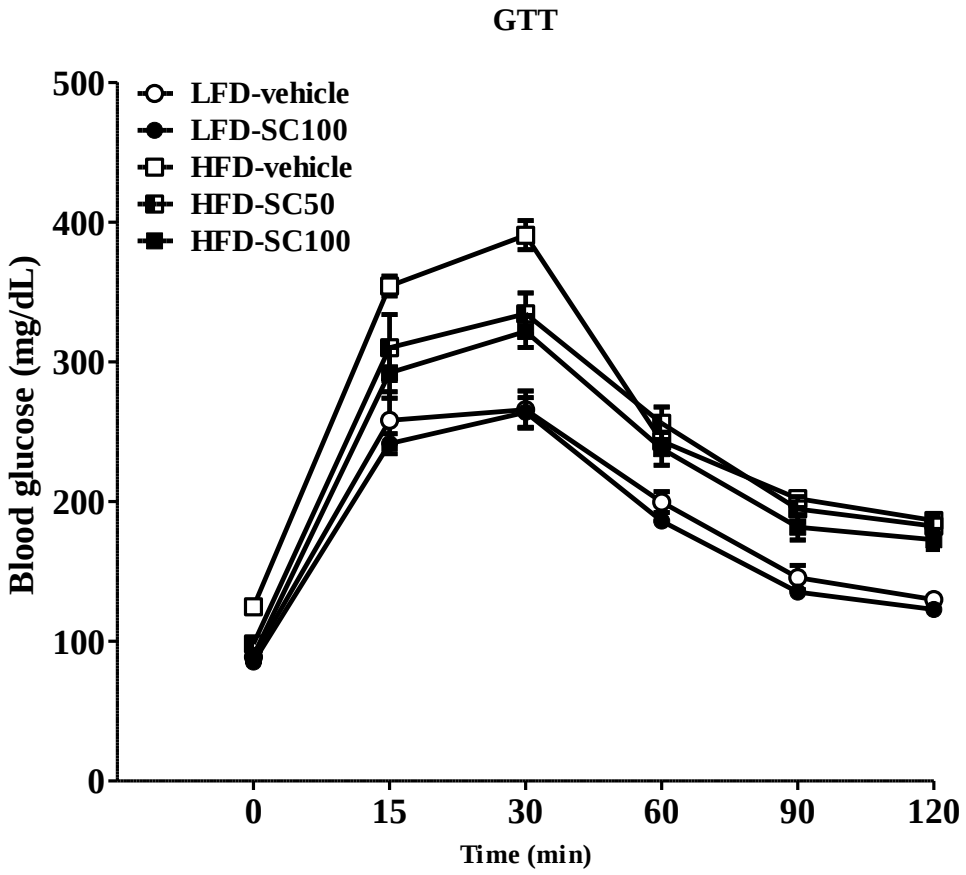

Figure 15. SC improved glucose tolerance in HFD-fed mice.

The blood glucose measurements at 0, 15, 30, 60, and 120 min after glucose injection by tail vein. The data were presented as the means ± SEM. GTT, glucose tolerance test; LFD, low fat diet; HFD, high fat diet; LFD-Vehicle, LFD fed mice treated with 0 mg/kg body weight SC; LFD-SC-100, LFD mice treated with 100 mg/kg body weight SC; HFD-Vehicle, HFD fed mice treated with 0 mg/kg body weight SC; HFD-SC-50, HFD fed mice treated with 50 mg/kg body weight SC;HFD-SC-100, HFD fed mice treated with 100 mg/kg body weight SC.

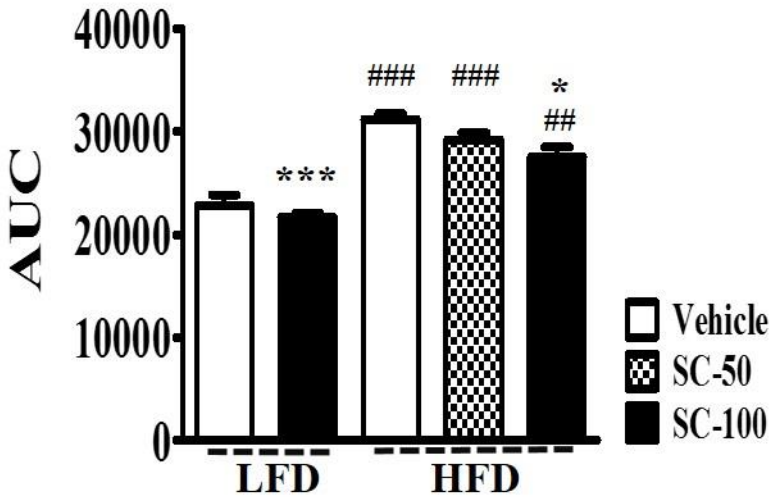

Figure 16. SC improved glucose tolerance in HFD-fed mice.

The AUC is the area under the curve of blood glucose curve calculated using Graphpad Prism program. The data were presented as the means ± SEM. * $p < 0.05$, ** $p < 0.01$, *** $p < 0.001$, compared to HFD-Vehicle; # $p < 0.05$, ## $p < 0.05$, ### $p < 0.001$, compared to LFD-Vehicle (ANOVA with dunnett's test). LFD, low fat diet; HFD, high fat diet; Vehicle, treated with 0 mg/kg body weight SC; SC-50, treated with 50 mg/kg body weight SC; SC-100, treated with 100 mg/kg body weight SC.

9. Effects of SC on energy expenditure and thermogenesis

Energy homeostasis is the result of a balance between energy intake and expenditure. Therefore, to detect energy intake and expenditure, we used the comprehensive lab animal monitoring system. As shown in Figure 17, the food intake was lower in the HFD groups than in the LFD groups, and there were no significant differences in food intake between the HFD-SC-100 and the HFD-vehicle groups or the LFD-SC-100 and the LFD-vehicle groups. In other words, SC administration did not affect the food intake in any of the groups. Energy consumption is hypothesized to increase if body fat and body weight are significantly lower than the energy intake. The energy consumption was measured using indirect calorimetry. The O_2 consumption of the HFD-SC-100 group was significantly higher than that of the HFD-vehicle group during both light and dark cycles, without differences in physical activity. In mice, heat generation is higher in the dark than the light. However, heat generation was significantly higher during both the daytime and the nighttime in the groups receiving 100 mg/kg SC (Figure 18).

BAT generates heat via energy consumption. As a result of measuring the surface heat of the living mice, the HFD-Vehicle was observed to have a smaller high-temperature region than the LFD-Vehicle. However, the HFD-SC-100 showed a higher-temperature region than that in the HFD-Vehicle, especially in the area where BAT was present. Active BAT can be identified by ^{18}F-FDG-PET/CT. In this study, PET/CT revealed that the ^{18}F-FDG signal was significantly higher in the interscapular region of the animals treated with 100 mg/kg SC (Figure 19).

Analysis of the standard uptake values demonstrated that 100 mg/kg SC administration increased the BAT activity. However, there were no significant differences between LFD-Vehicle and LFD-SC-100 groups in VO2, heat, and ^{18}F-FDG uptake.

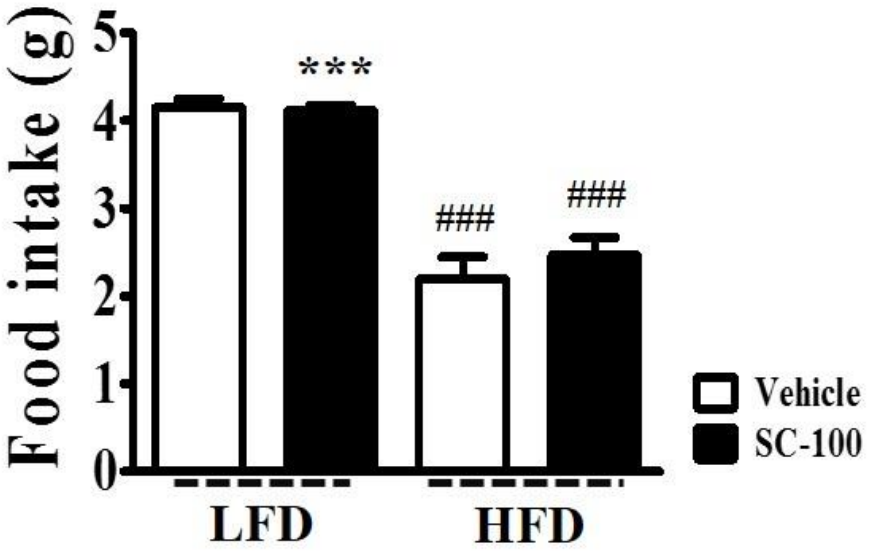

Figure 17. SC does not affect food intakes.

The data were presented as the means ± SEM. * $p < 0.05$, ** $p < 0.01$, *** $p < 0.001$, compared to HFD-Vehicle; # $p < 0.05$, ## $p < 0.05$, ### $p < 0.001$, compared to LFD-Vehicle. LFD, low fat diet; HFD, high fat diet; Vehicle, treated with 0 mg/kg body weight SC; SC-100, treated with 100 mg/kg body weight SC.

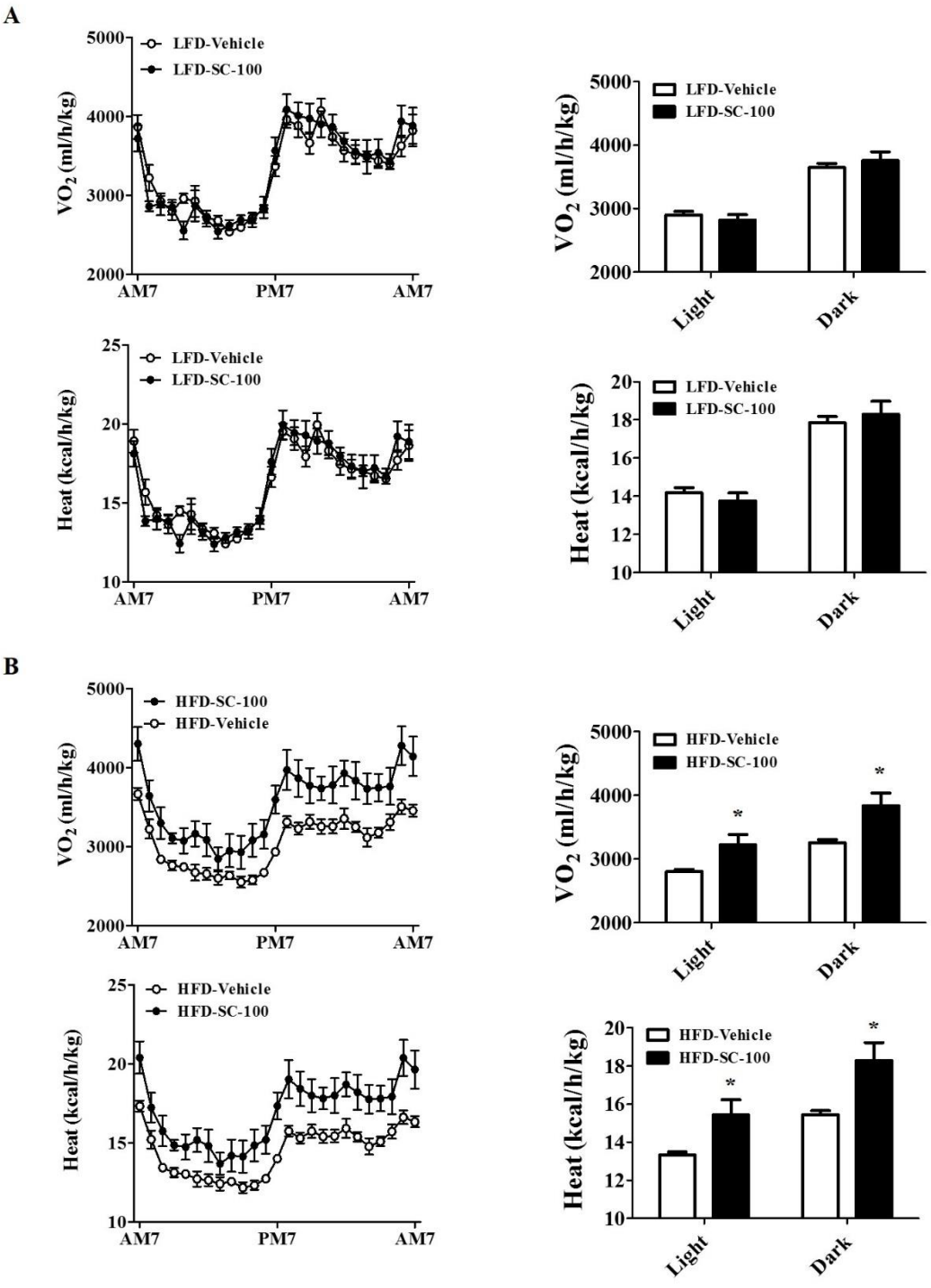
A
LFD-Vehicle
LFD-SC-100
VO_2 (ml/h/kg)
Heat (kcal/h/kg)
AM7
PM7
AM7
Light
Dark
B
HFD-SC-100
HFD-Vehicle
*

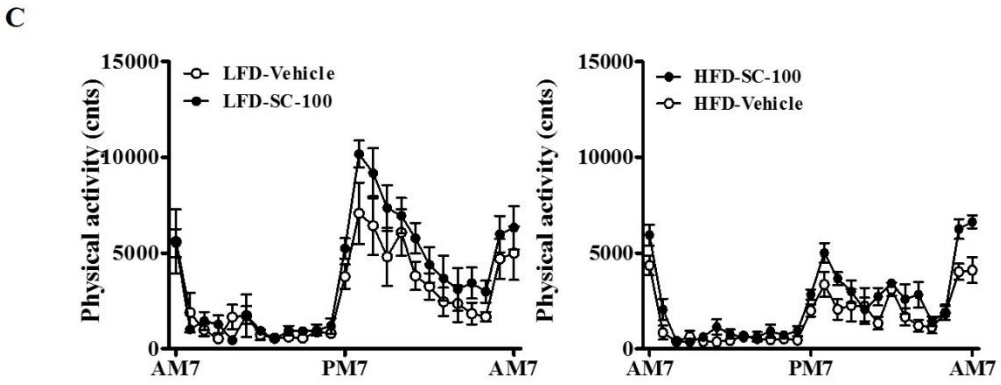

Figure 18. SC increase metabolic rate in HFD-fed mice.

Metabolic rate, heat and physical activity were observed when the experimental mice were housed in indirect calorimetry for 72 hours. The data were presented as the means ± SEM. * $p < 0.05$, ** $p < 0.01$, *** $p < 0.001$, compared to HFD-Vehicle; # $p < 0.05$, ## $p < 0.05$, ### $p < 0.001$, compared to LFD-Vehicle. VO_2, volume of oxygen consumed; LFD, low fat diet; HFD, high fat diet; LFD-Vehicle, LFD fed mice treated with 0 mg/kg body weight SC; LFD-SC-100, LFD mice treated with 100 mg/kg body weight SC; HFD-Vehicle, HFD fed mice treated with 0 mg/kg body weight SC; HFD-SC-100, HFD fed mice treated with 100 mg/kg body weight SC.

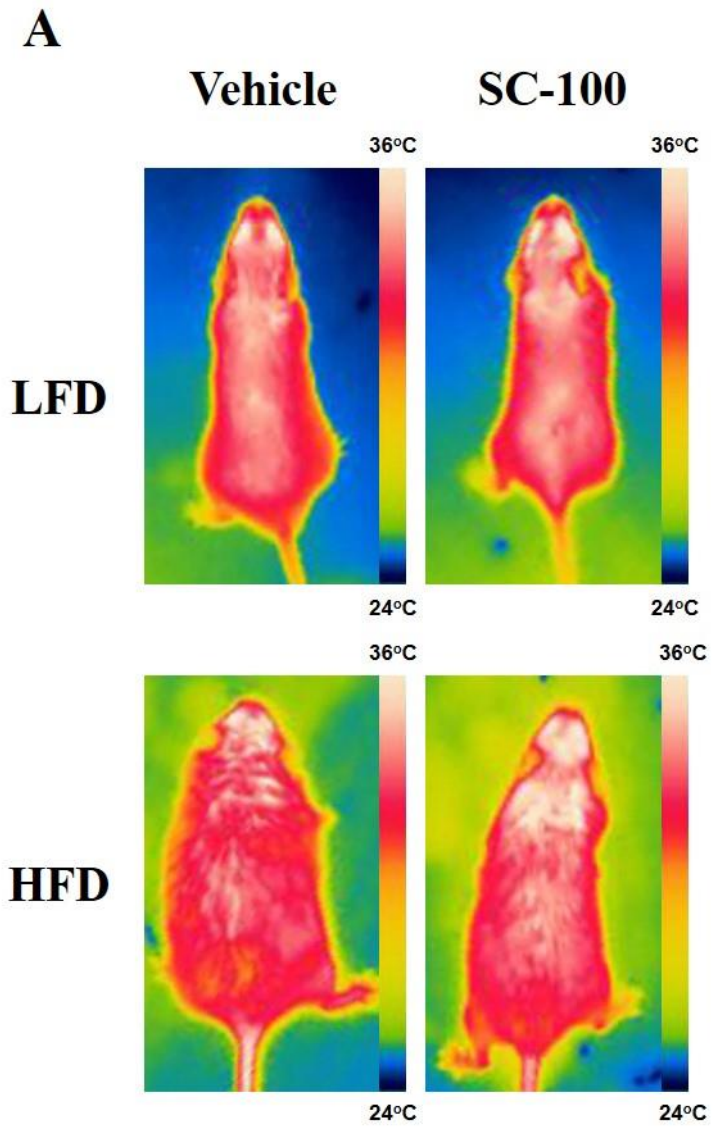

(continue)

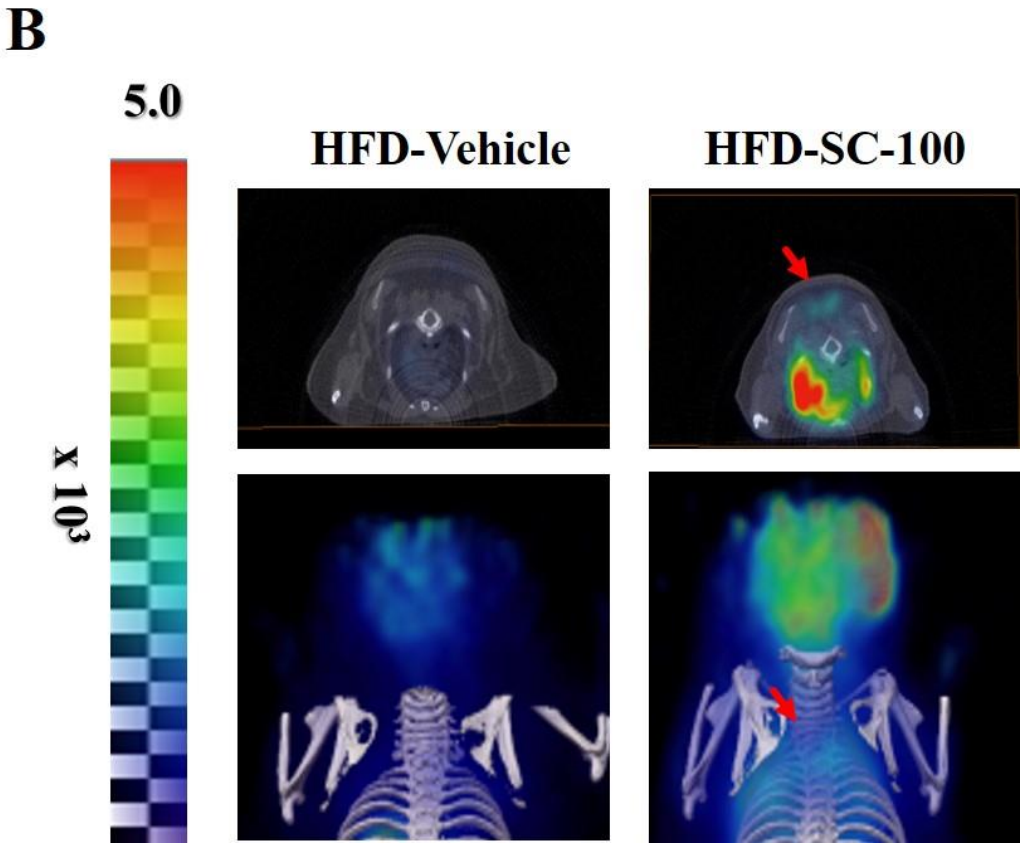
B
5.0
x 10³
HFD-Vehicle
HFD-SC-100

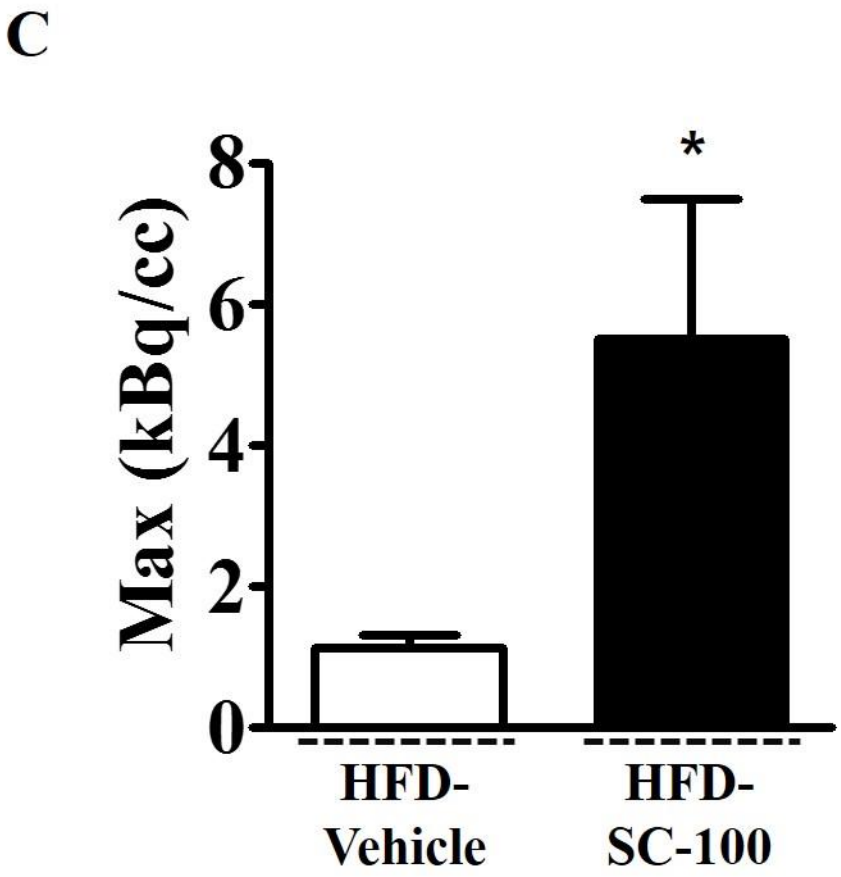

Figure 19. SC increases ^{18}F-FDG uptake in the BAT of HFD-fed mice.

A photograph was taken with a thermal digital camera to measure the heat generation site (A). The activity of BAT in experimental animal after 14 weeks of HFD feeding was assessed by PET-computed tomography (CT). 3-Demensional reconstructed positron emission tomography/computed tomography imaging with ^{18}F-FDG (B) and quantification of ^{18}F-FDG uptake in BAT (C). Red arrows indicate the activated BAT. The data were presented as the means ± SEM. HFD-SC-100 was statistically different compared to HFD-Vehicle. LFD, low fat diet; HFD, high fat diet; HFD-Vehicle, HFD fed mice treated with 0 mg/kg body weight SC; HFD-SC-100, HFD fed mice treated with 100 mg/kg body weight SC.

10. SC increases thermogenesis-related gene and protein expression in BAT

BAT morphology evaluated after 14 weeks of HFD feeding in mice revealed that the size of lipid droplets was increased in the HFD-vehicle group compared with that in the LFD-vehicle group and decreased in the HFD-SC-100 group compared with that in the HFD-vehicle group (Figure 20.A). The expression of UCP1, a classical marker of BAT function, was lower in the HFD-vehicle group than in the LFD-vehicle group and higher in the HFD-SC-100 group than in the HFD-Vehicle group (Figure 20. B). Analysis of the genes controlling energy expenditure and thermogenic signaling in BAT revealed that the expressions of thermogenesis-associated transcription factors UCP1, TFAM, PREM16, Dio2, Cidea, GLUT1, GLUT4, PPARα, PPARγ, and ATGL were significantly activated in BAT of the HFD-SC-100 group compared to the HFD-vehicle group. The expressions of the classical BAT marker genes NRF1 and PGC1α were activated by 100 mg/kg SC administration in the HFD group (Figure 21). Finally, the protein levels of UCP1 and pAMPK were augmented by 100 mg/kg SC administration in mice receiving HFD (Figure 22).

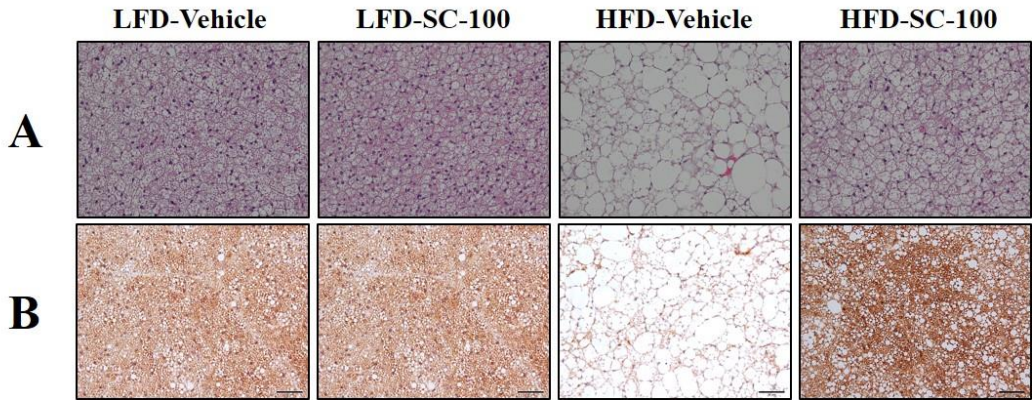

Figure 20. Morphological analysis in BAT.

The paraffin section of BAT was stained with H&E (A) and immunostained with UCP1 (B). Subsequently, the stained tissue was photographed under a microscope (magnification *400). LFD, low fat diet; HFD, high fat diet; LFD-Vehicle, LFD fed mice treated with 0 mg/kg body weight SC; LFD-SC-100, LFD mice treated with 100 mg/kg body weight SC; HFD-Vehicle, HFD fed mice treated with 0 mg/kg body weight SC; HFD-SC-100, HFD fed mice treated with 100 mg/kg body weight SC.

A

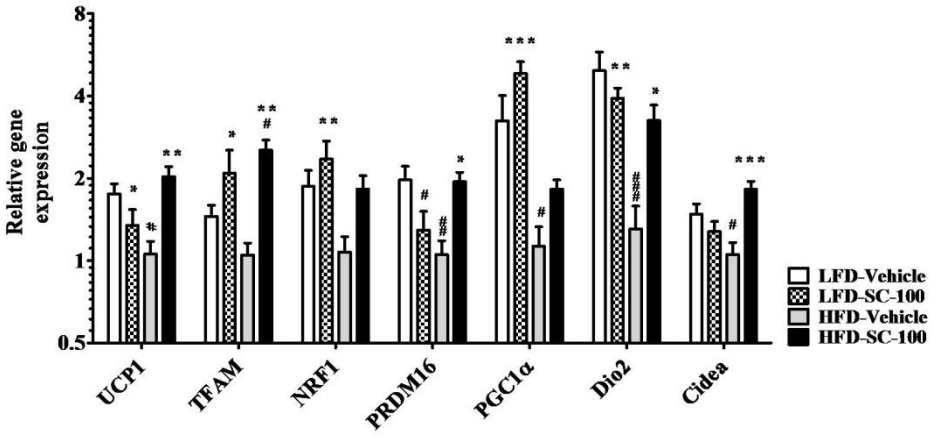
Relative gene expression
8
4
2
1
0.5
UCP1
TFAM
NRF1
PRDM16
PGC1α
Dio2
Cidea
LFD-Vehicle
LFD-SC-100
HFD-Vehicle
HFD-SC-100

(continue)

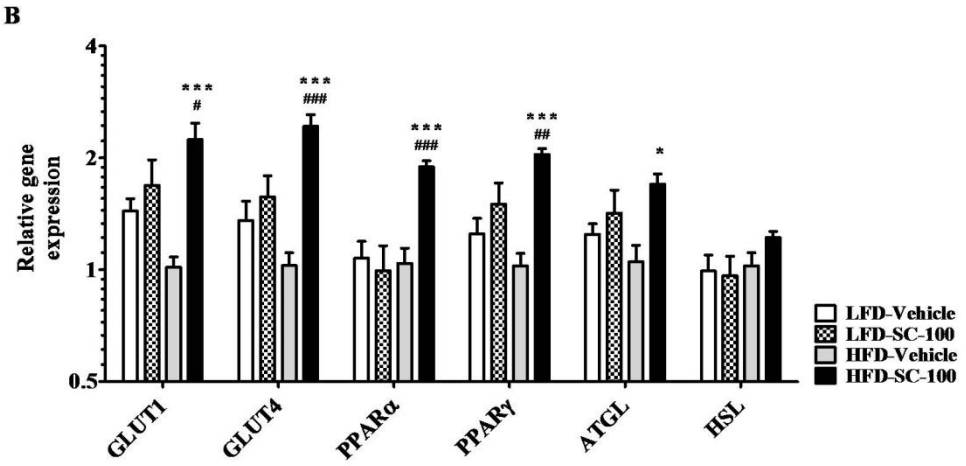

Figure 21. SC increases thermogenesis related gene expression in the BAT of HFD-fed mice.

The data were presented as the means ± SEM. * $p < 0.05$, ** $p < 0.01$, *** $p < 0.001$, compared to HFD-Vehicle; # $p < 0.05$, ## $p < 0.05$, ### $p < 0.001$, compared to LFD-Vehicle (ANOVA with dunnett's test). LFD, low fat diet; HFD, high fat diet; LFD-Vehicle, LFD fed mice treated with 0 mg/kg body weight SC; LFD-SC-100, LFD mice treated with 100 mg/kg body weight SC; HFD-Vehicle, HFD fed mice treated with 0 mg/kg body weight SC; HFD-SC-100, HFD fed mice treated with 100 mg/kg body weight SC

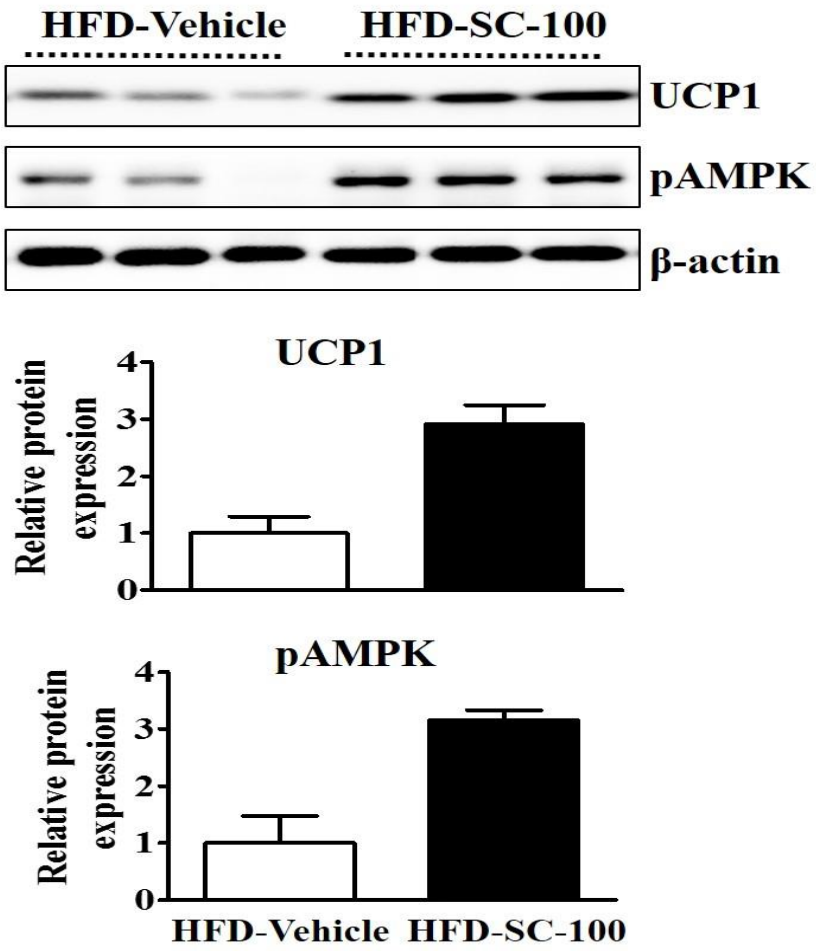

Figure 22. SC increases UCP1 and pAMPK protein expression in the BAT of HFD-fed mice.

Western blotting was used to analyze the pAMPK and UCP1 protein expression in sWAT of high fat diet fed mice. β-tubulin was used as a normalized control and the relative protein expression was presented as the ratio of the HFD-Vehicle. The data were presented as the means ± SEM. HFD-Vehicle, HFD fed mice treated with 0 mg/kg body weight SC; HFD-SC-100, HFD fed mice treated with 100 mg/kg body weight SC.

11. SC enhances UCP1 expression in IBA through the AMPK pathway

AMPK signaling is one of the major factors controlling thermogenesis in BAT. To determine whether SC had a direct effect on the development of thermogenesis, differentiated IBA cells were treated with the SC, which demonstrated that the heat generation-related factor UCP1 was significantly increased in SC-treated cells and that AMPK phosphorylation was time-dependent (Figure 23). To determine whether UCP1 induction were directly mediated by AMPK activation, expressions of the AMPK α 1 and 2 subunits were knocked down by specific siRNAs transfected into IBA cells, which were previously reported to be a suitable model for BAT-selective gene studies (Aune et al., 2013). AMPK protein levels were decreased with transfection of siRNAs against the AMPK α 1 and 2 subunits. Treatment of these cells with the SC led to a reduction in UCP1 protein expression (Figure 24). These results suggest that SC enhances heat generation through AMPK pathway activation in brown adipocytes.

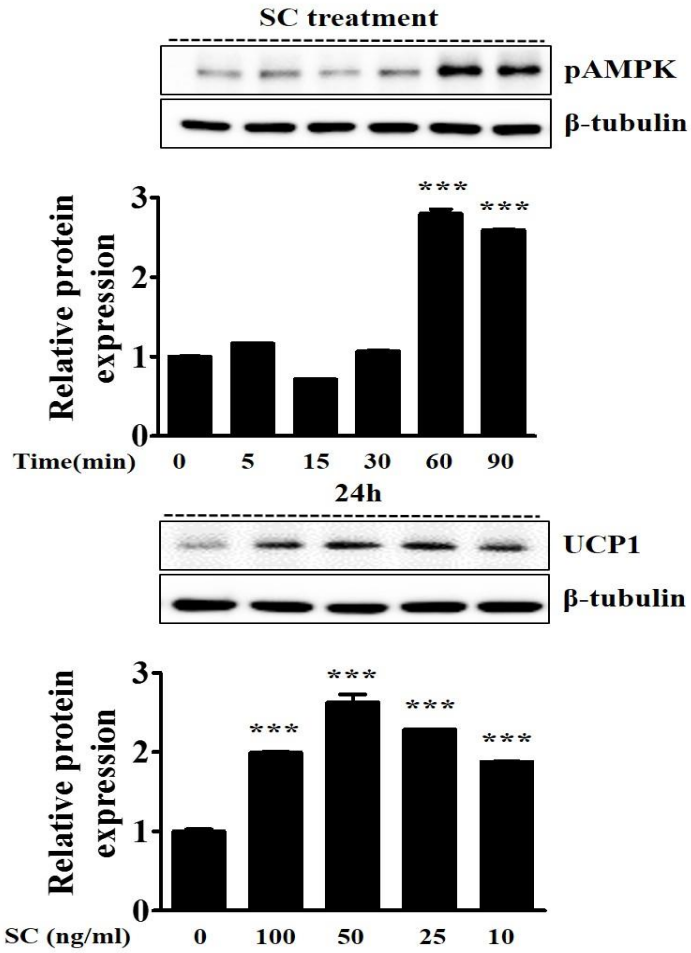

Figure 23. SC increase pAMPK and UCP1 protein expression in the differentiated IBA.

100 ng/ml dose of SC were treated with differentiated IBA and proteins were extracted at 0, 15, 30, 60, and 90 min and pAMPK protein expression were analyzed. The UCP1 protein expression of differentiated IBA after 24h of treatment with or without SC also analyzed. β-tubulin was used as a normalized control, and the relative protein expression was presented as a relative levels of 0. The data were presented as the means ± SEM. *$p < 0.05$, **$p < 0.01$, ***$p < 0.001$, compared to "0" exposure without SC treatment.

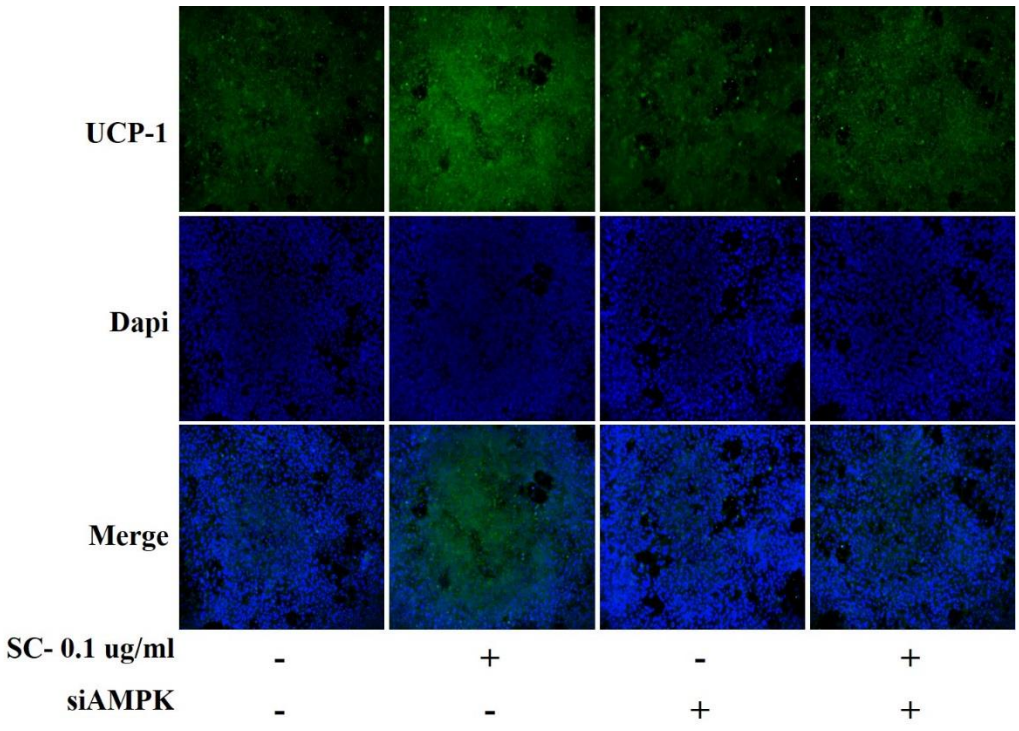

Figure 24. SC increase UCP1 expression in differentiated IBA through AMPK activation

IBA were transfected with AMPK siRNA for 24h and differentiated via differentiation meduim. Differentiated IBA was treated with or without IBA for 24h and then immunostaining was performed. The UCP1 (green) expression was observed using microscopy and UCP1 and dapi (blue) overlapped.

12. SC promotes browning in sWAT of mice with HFD-induced obesity

To examine the browning effect of SC on white adipocytes, we performed H&E and immunohistochemistry staining for UCP1 antibody and evaluated thermogenesis-associated gene and protein levels in the sWAT of mice. As shown in Figure 25A, the size of lipid droplets was increased in the HFD-vehicle group compared with that in the LFD-vehicle group and decreased in the HFD-SC-100 group compared with the HFD-vehicle group. UCP1-positive adipocytes were markedly increased in the HFD-SC-100 group compared with the HFD-vehicle group (Figure 25B). The UCP1 and PGC1α gene expression levels were also significantly increased in the HFD-SC-100 group compared with those in the HFD-vehicle group. However, TFAM, NRF1, PRDM16, Dio2, and Cidea gene expressions did not increase in HFD-SC-100 group compared with those in the HFD-Vehicle group. The expression levels of thermogenesis-associated genes were not significantly different between the LFD-vehicle and the LFD-SC-100 group (Figure 26). Finally, pAMPK and UCP1 protein levels were increased in the HFD-SC-100 group compared with those in the HFD-vehicle group. Altogether, these results indicated that SC administration promoted browning in the sWAT of mice with HFD-induced obesity (Figure 27).

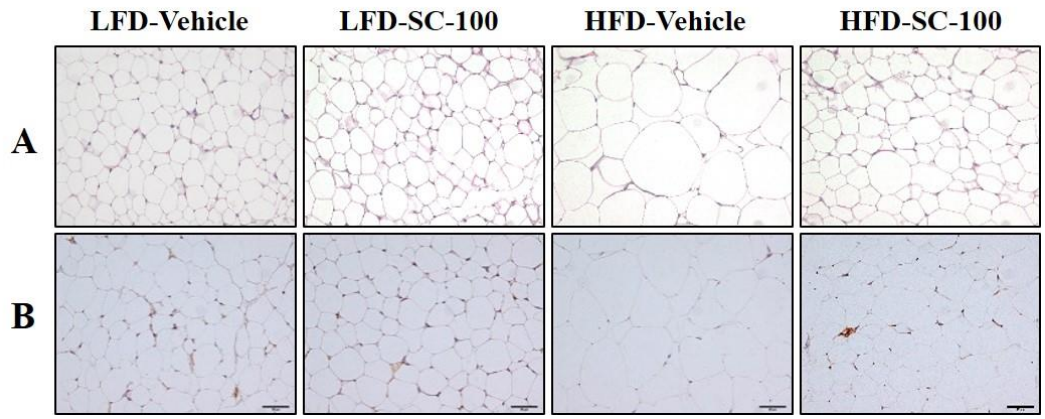

Figure 25. Morphological analysis of H&E and immunostained with UCP1 in sWAT.

The paraffin section of sWAT was stained with H&E (A) and immunostained with UCP1-antibody (B). Subsequently, the stained tissue was photographed under a microscope (magnification *400, scale bar =50 um). sWAT, subcutaneous adipose tissue; UCP1, uncoupling protein 1; LFD, low fat diet; HFD, high fat diet; LFD-Vehicle, LFD fed mice treated with 0 mg/kg body weight SC; LFD-SC-100, LFD mice treated with 100 mg/kg body weight SC; HFD-Vehicle, HFD fed mice treated with 0 mg/kg body weight SC; HFD-SC-100, HFD fed mice treated with 100 mg/kg body weight SC.

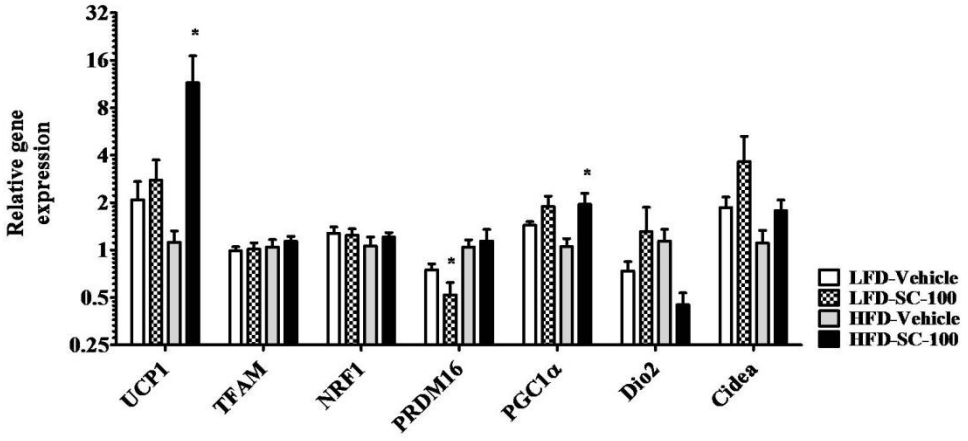

Figure 26. SC increases thermogenesis related gene expression in the sWAT of HFD-fed mice.

The data were presented as the means ± SEM. * $p < 0.05$, ** $p < 0.01$, *** $p < 0.001$, compared to HFD-Vehicle; # $p < 0.05$, ## $p < 0.05$, ### $p < 0.001$, compared to LFD-Vehicle (ANOVA with dunnett's test). LFD, low fat diet; HFD, high fat diet; LFD-Vehicle, LFD fed mice treated with 0 mg/kg body weight SC; LFD-SC-100, LFD mice treated with 100 mg/kg body weight SC; HFD-Vehicle, HFD fed mice treated with 0 mg/kg body weight SC; HFD-SC-100, HFD fed mice treated with 100 mg/kg body weight SC

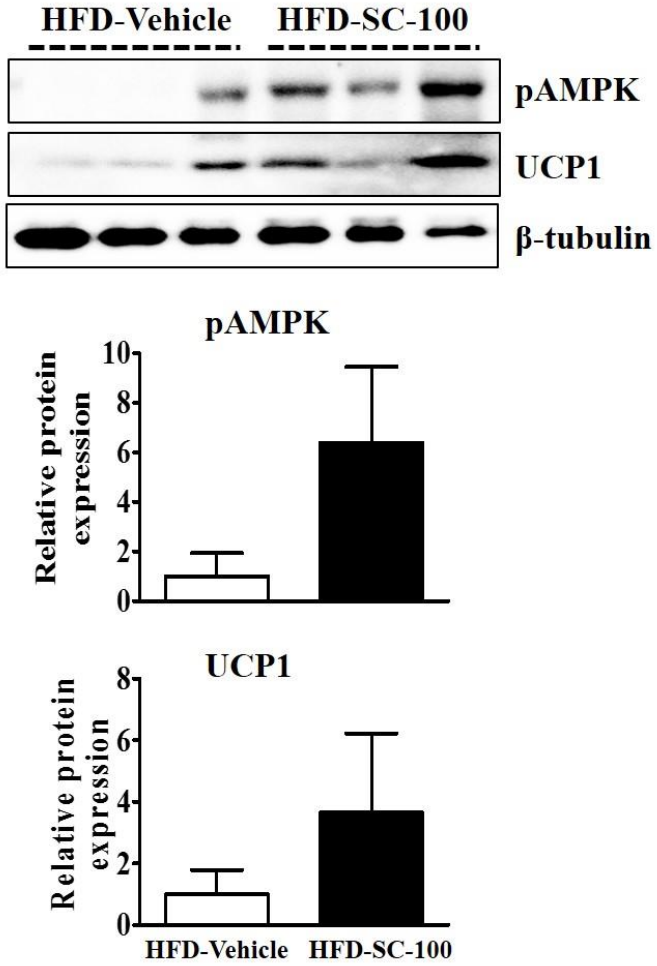

Figure 27. SC increases pAMPK and UCP1 protein expression in the sWAT of HFD-fed mice.

The data were presented as the means ± SEM. LFD, low fat diet; HFD, high fat diet; LFD-Vehicle, LFD fed mice treated with 0 mg/kg body weight SC; LFD-SC-100, LFD mice treated with 100 mg/kg body weight SC; HFD-Vehicle, HFD fed mice treated with 0 mg/kg body weight SC; HFD-SC-100, HFD fed mice treated with 100 mg/kg body weight SC.

13. Effect of SC on inflammation in epithelial white adipose tissue

For analysis of the genes controlling energy expenditure and thermogenic signaling in epididymal adipose tissue, the expressions of thermogenesis-associated transcription factors UCP1, TFAM, PREM16, Dio2, Cidea, and NRF1 were detected. Unlike BAT and sWAT, there was no significant difference in the expression of thermogenesis associated transcription factor between the HFD-Vehicle group and HFD-SC-100 group (Figure 28). Obesity-related inflammatory diseases are associated with increased inflammatory cytokines and decreased adiponectin (Ibrahim, 2010). As shown in Figure 29, there were significant increases in inflammatory cytokines such as FA/80, CD11c, MCP-1, and leptin gene expressions in the HFD-Vehicle group compared with those in the LFD group, and the adiponectin gene expression was decreased in the HFD-Vehicle group compared with in the LFD- group. However, inflammatory cytokines were significantly decreased in the HFD-SC-100 group compared with the HFD-Vehicle group. In particular, the HFD-SC-100 group showed a significant increase in adiponectin gene expression compared with HFD-vehicle.

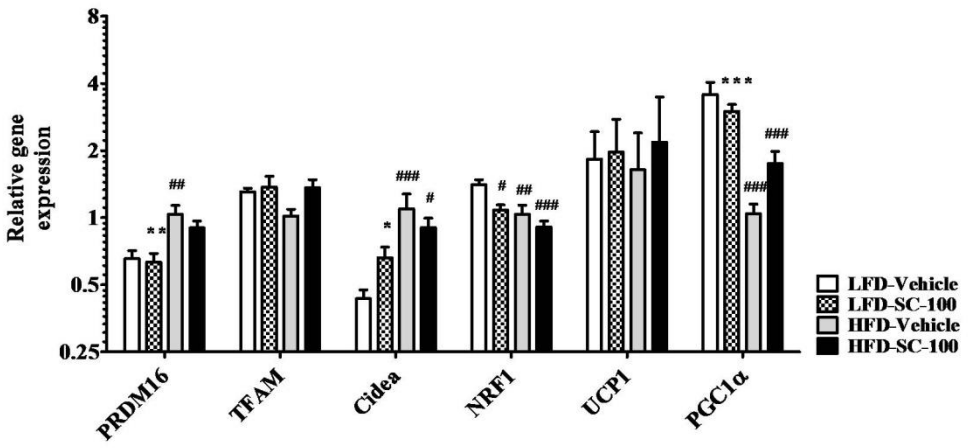

Figure 28. SC does not affect thermogenesis associated gene expression in epithelial white adipose tissue.

The gene expressions were examined by real-time PCR and the gene expression data were normalized to 36B4 and analyzed using $2(^{-\Delta\Delta CT})$ method. The data were presented as the means ± SEM. * $p < 0.05$, ** $p < 0.01$, *** $p < 0.001$, compared to HFD-Vehicle; # $p < 0.05$, ## $p < 0.05$, ### $p < 0.001$, compared to LFD-Vehicle (ANOVA with dunnett's test). LFD, low fat diet; HFD, high fat diet; LFD-Vehicle, LFD fed mice treated with 0 mg/kg body weight SC; LFD-SC-100, LFD mice treated with 100 mg/kg body weight SC; HFD-Vehicle, HFD fed mice treated with 0 mg/kg body weight SC; HFD-SC-100, HFD fed mice treated with 100 mg/kg body weight SC.

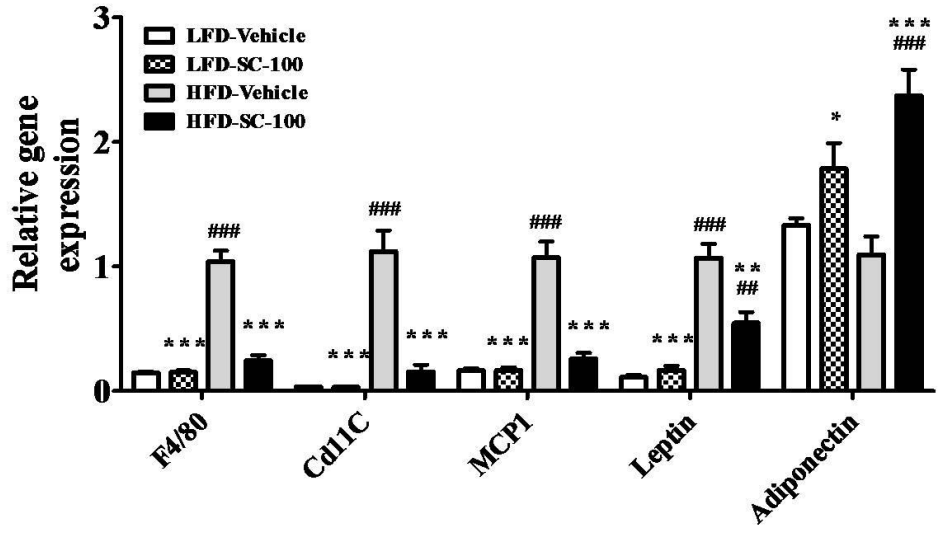

Figure 29. SC ethanol extract inhibits inflammation in epithelial white adipose tissue.

The gene expressions were examined by real-time PCR and the gene expression data were normalized to 36B4 and analyzed using $2(^{-\Delta\Delta CT})$ method. The data were presented as the means ± SEM. * $p < 0.05$, ** $p < 0.01$, *** $p < 0.001$, compared to HFD-Vehicle; # $p < 0.05$, ## $p < 0.05$, ### $p < 0.001$, compared to LFD-Vehicle (ANOVA with dunnett's test). LFD, low fat diet; HFD, high fat diet; LFD-Vehicle, LFD fed mice treated with 0 mg/kg body weight SC; LFD-SC-100, LFD mice treated with 100 mg/kg body weight SC; HFD-Vehicle, HFD fed mice treated with 0 mg/kg body weight SC; HFD-SC-100, HFD fed mice treated with 100 mg/kg body weight SC.

14. SC enhances the expression of UCP1 via the AMPK pathway in 3T3-L1 cells

A previous study has shown that UCP1 expression increases following AMPK activation in differentiated 3T3-L1 cells (Choi J H et al., 2016). To determine whether SC had a direct effect on UCP1 and PGC1α expression in WAT, differentiated 3T3-L1 cells were treated with SC (Figure 30), revealing that the thermogenesis-associated factors UCP1 and PGC1α were significantly increased and that there was a dose-dependent increase in AMPK phosphorylation. To determine whether UCP1 and PGC1α were induced by AMPK activation, the expression of the AMPK α 1 and 2 subunits were knocked down by specific siRNAs transfected into IBA cells. The protein levels of both AMPK subunits were decreased with siRNA transfection. Importantly, SC treatment of cells transfected with AMPK siRNA exhibited decreased UCP1 and PGC1α protein expression, compared with the untransfected differentiated 3T3-L1 cells. These results suggested that SC enhanced browning through AMPK pathway activation in white adipocytes.

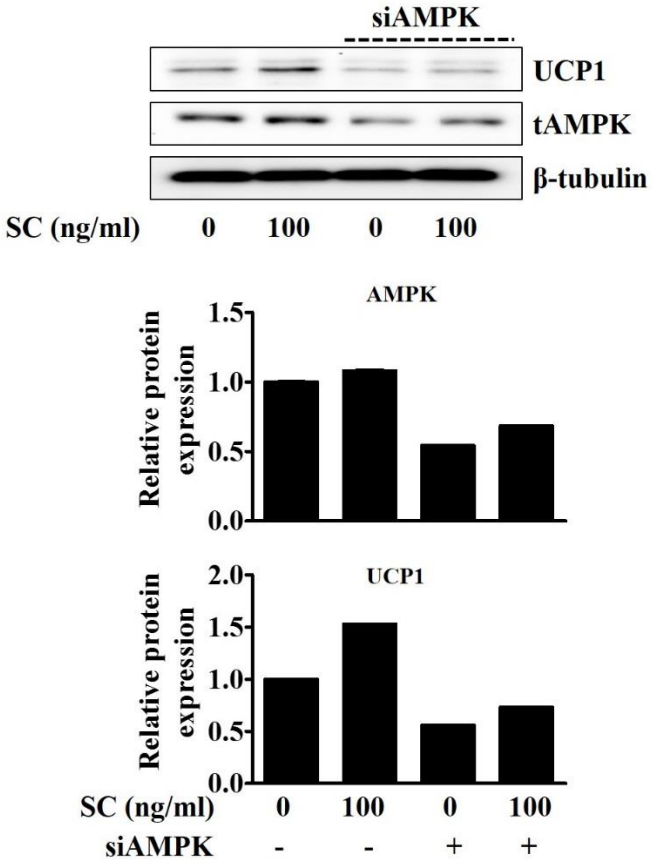

Figure 30. SC increases UCP1 expression in differentiated 3T3-L1 cells through AMPK activation.

3T3-L1 cells were transfected with siAMPK for 24h and differentiated via differentiation meduim. Differentiated 3T3-L1 cells was treated with or without SC for 24h and then protein was extracted. β-tubulin was used as a normalized control, and the relative protein expression was presented as a relative levels of non-treated differentiated cells.

15. Identification of phytochemical constituents

SC was were analyzed by LC-DAD-MS. In Figure 31, four flavonoid (i.e. rutin, isoquercitrin, quercitrin, quercetin), 2 phenolics (i.e. cholorogenic acid, neocholorogenic acid), 1 lignan (i.e. sauchinone) were identified in comparison with retention time and mass spectrum of authentic standards. The retention time of neocholorogenic acid, cholorogenic acid, rutin, isoquercitrin, quercitrin, quercetin, sauchinone were 4.65, 5.12, 6.55, 6.75, 7.54, 9.58, and 17.3, respectively (Table 3). These data are consistent with Chen et al. (2010).

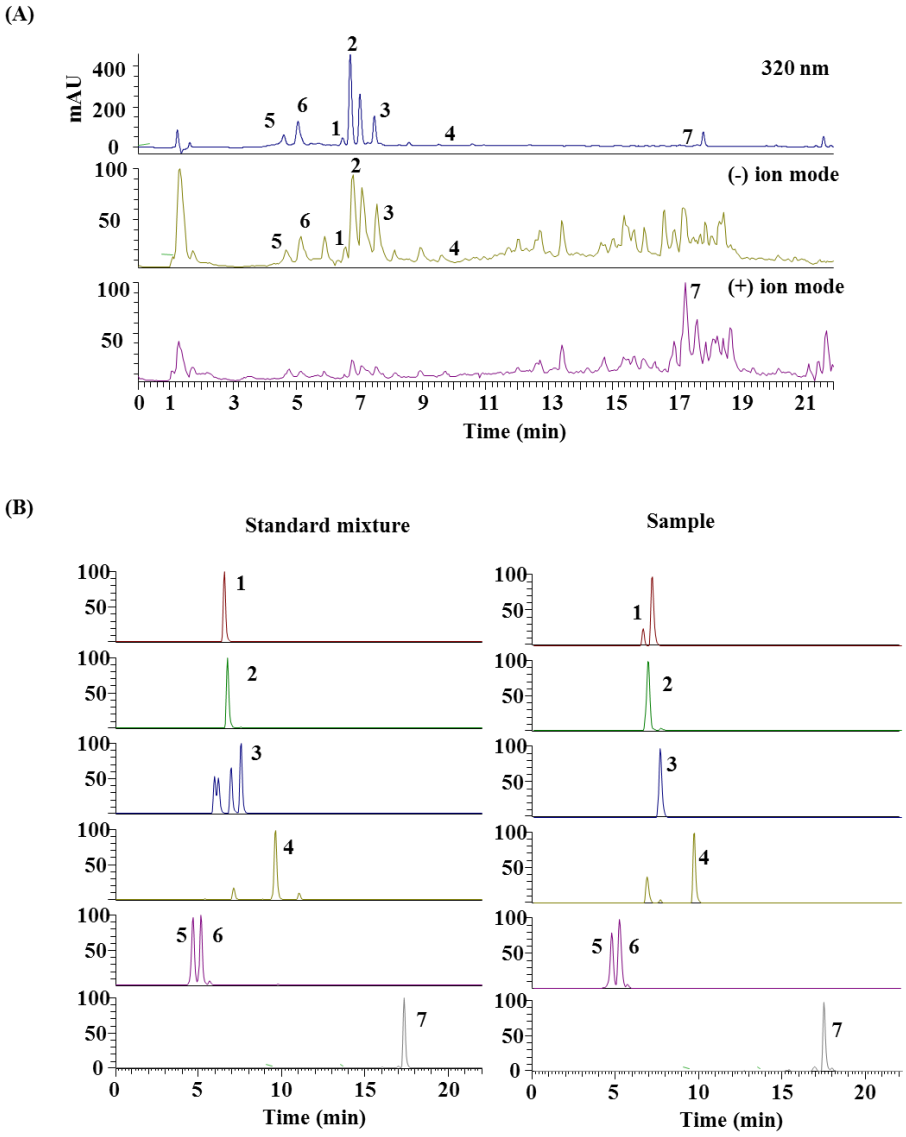

Figure 31. LC-DAD-MS of identified phytochemicals in SC.

HPLC and total ion chromatogram of SC (20 mg/mL) (A), extract ion chromatogram of SC (B). Rutin (1), isoquercitrin (2), quercitrin (3), quercetin (4), cholorogenic acid (5), neocholorogenic acid (6), sauchinone (7).

Table 3. Phytochemicals identified in SC by liquid chromatography-mass spectrometry.

Compound	Retention time (Min)	Chemical formula	Adduct	Calculated (*m/z*)	Measured (*m/z*)	Error (ppm)
Neochlorogenic acid	4.65	$C_{16}H_{18}O_9$	$[M-H]^-$	353.0878	353.0874	-1.155
Chlorogenic acid	5.12	$C_{16}H_{18}O_9$	$[M-H]^-$	353.0871	353.0873	-1.500
Rutin	6.55	$C_{27}H_{30}O_{16}$	$[M-H]^-$	609.1461	609.1455	-1.089
Isoquercitrin	6.75	$C_{21}H_{20}O_{12}$	$[M-H]^-$	463.088	463.0877	-1.063
Quercitrin	7.54	$C_{21}H_{20}O_{11}$	$[M-H]^-$	447.0933	447.0926	-1.543
Quercetin	9.58	$C_{15}H_{10}O_7$	$[M-H]^-$	301.0354	301.0350	-1.352
Sauchinone	17.3	$C_{20}H_{20}O_6$	$[M+H]^+$	357.1333	357.1324	-2.364

Discussion

SC is a traditional herbal medicine that has been used in inflammatory disorders. SC has been shown to exert anti-obesity effects in animal models of HFD-induced obesity (Yun et al., 2007) and to inhibit adipocyte differentiation in 3T3-L1 cells (Yu et al., 2008). However, the mechanism underlying its anti-obesity effects remains unclear. In the current study, we have verified the anti-obesity effects of SC in HFD-fed mice and investigated the underlying mechanism of the action of SC using IBA and 3T3-L1 cells.

A previous study has shown that treatment with SC inhibits lipid accumulation by inhibiting adipogenic factors, such as C/EBPα and PPARγ (Yu et al., 2008), but its upstream mechanism has not yet been reported. In the current study, the SC treatment of 3T3-L1 cells significantly inhibited lipid formation and significantly decreased the expression of adipogenic factors including ACC, FAS, SREBP1, PPARγ, and C/EBPα; compared to untreated differentiated cells. To elucidate the mechanism of inhibitory effects during adipogenesis, the protein expression in the early stage of differentiation was detected. In the current study, SC led to increased phosphorylation of AMPK and ACC in the early stage of differentiation. AMPK regulates preadipocyte differentiation, fatty acid oxidation, and fatty acid synthesis (Kumar et al., 2006). The AMPK pathway was has been reported to be responsible for the inhibition of adipocyte differentiation by natural compounds such as epigallocatechin gallate (Moon et al., 2007), genistein, capsaicin (Hwang et al., 2005), and resveratrol (Wang S et al., 2015). The present study also found that the inhibitory effect of the SC on lipogenesis was significantly attenuated in siAMPK-

transfected 3T3-L1 cells. These results indicate that SC activated AMPK signaling and that the AMPK pathway activation is a significant contributor to the suppression of lipogenesis in adipocytes.

Animal models of diet-induced obesity (DIO) are important tools for understanding the relationship between high-calorie Western diets and obesity development. In DIO, animals are fed a long-term HFD, which leads to obesity, with several concomitant abnormalities in glucose and lipid metabolism such as impaired glucose tolerance, hyperglycemia, hyperlipidemia, and hyperinsulinemia (Wang C Y et al., 2012). In the current study, mice that had been fed HFD were administered the SC. The results revealed that the HFD-fed mice exhibited significantly higher body weight gain, total fat content, body fat ratio, and hepatic lipid accumulation than LFD-fed mice. However, these changes were significantly improved by the administration of 100 mg/kg SC in HFD-fed mice. In addition, the impaired glucose metabolism, as evidenced by increased fasting glucose and insulin and impaired glucose tolerance, and the altered lipid metabolism, as evidenced by increased FFA, leptin, and cholesterol metabolism (TC and LDL-C), induced by HFD, were significantly improved by administering SC. These results suggest that SC has a significant effect on improving obesity induced by HFD, which adds to the results of a precious studies that showed that SC improved blood lipids profiles, and tissue lipid contents in obese rats as induced by HFD.

The disparity in energy supply and consumption is a major cause of obesity. There have been many efforts to treat obesity by suppressing appetite. However, a representative appetite suppressant, sibutramine, has been withdrawn from the

market due to cardiovascular side effects, and, currently, FDA-approved appetite suppressants are also unavailable for long periods due to serious side effects. The increase in energy consumption is attracting attention as a target of new obesity treatment, but there is no approved drug to treat obesity by increasing energy consumption. In the current study, the HFD-SC-100 group exhibited significantly decreased body weight gain and total fat weight, despite the lack of any reduction in food intake. The reduction in fat mass without changing lean mass despite maintaining the same calorie intake suggests the possibility of increased energy expenditure. Energy expenditure is associated with basal metabolism, feeding, physical activity, and thermogenesis (Speakman, 2013). In the indirected calorimetry study, SC administration increased oxygen consumption and heat production in HFD-fed mice without significant increase in physical activity. These results suggest that SC administration may increase the energy consumption by increasing heat generation. Whether this heat production was related to the activity of BAT was investigated by measuring ^{18}F-FDG uptake in a living state, and thermogenesis-related factor expression was analyzed by various methods after autopsy. The results of this study showed that the uptake of ^{18}F-FDG and UCP1, PGC1α, PRDM16, Dio2, Cidea, and TFAM were increased in mice that were fed high-fat diets with SC administration. These results suggest that BAT activity is improved by SC.

BAT thermogenesis as an appealing way to treat or prevent obesity. BAT activation induced in mice has been reported to promote energy expenditure, reduce adiposity, and protect mice from diet-induced obesity (Lowell et al., 1993; Ghorbani et al., 1997; Cypess et al., 2010). BAT dissipates energy in the form of heat by

uncoupling fatty acid oxidation from ATP production via UCP1 in the mitochondria and protects against obesity (Shen et al., 2014). FFA is major energy source of heat production; the activation of BAT leads to the lipolysis of intracellular TG-filled lipid droplets by ATGL and HSL and the subsequent release of FFA (Thoonen et al., 2016). In this study, ATGL gene expression was significantly increased in SC-treated HFD mice. The PPARγ, which contributed to FFA uptake in adipose tissue, was also increased in SC-treated HFD mice. These results suggest the possibility that SC administration increases the FFA uptake in BAT from the blood and increases FFA release by increasing lipolysis to increase the concentration of FFA. FFA was reported to be metabolized by β-oxidation in mitochondrial matrix and/or it activated UCP1. Our data showed that SC treatment upregulated PGC1α and PPARα; these results suggest that SC increases the FFA oxidation in BAT, which contributes to heat production.

The ^{18}F-FDG uptake using PET-CT was a useful method for the BAT activity (Baba et al., 2010); in addition, FDG accumulation is reported as caused by increased glucose utilization and the transport of FDG across the cell membrane is related to GLUT expression (Brown et al., 1999). BAT displays high rates of glucose uptake; GLUT1 activation and GLUT4 expression and translocation are major positive regulators of BAT glucose uptake (Festuccia et al., 2011) and GLUT expression correlates with heat production. Low temperature exposure has been reported to increase GLUT1 and GLUT4 expression in BAT compared to other organs (Bartelt et al., 2011), and it has been suggested that BAT may serve as an important glucose sink to improve insulin resistance and lower blood glucose levels (Vallerand et al., 1987; Townsend et al., 2014). In this study, GLUT1 and

GLUT4 gene expressions were significantly expressed in the BAT of SC-administered HFD mice. The expressions of PPARα and PPARγ genes related to glucose uptake and oxidation were also increased in the BAT of HFD mice treated with SC. These results suggest that the administration of SC may improve hyperglycemia and hyperinsulinemia induced by HFD due to the increased glucose uptake of BAT.

Sustained activation of AMPK stimulated fatty acid oxidation (Kumar et al., 2006; Luo B et al., 2007) and mitochondria biogenesis (Orci et al., 2004). Previous studies have reported that AICAR stimulates the expression of PPARα, PPARγ, and PGC1α (Gaidhu et al., 2009; Ahmadian et al., 2011), and these factors are reported to have a beneficial effect on BAT activity. AMPK activation was recently linked to BAT function. For example, resveratrol was shown to enhance brown adipocyte formation and upregulate UCP1 and PRDM16 via AMPK activation (Wang S et al., 2017). Additionally, berberine reportedly increased UCP1 expression in BAT, which was previously shown to involve AMPK and PGC1α (Zhang Z et al., 2014). In the current study, phosphorylated AMPK levels were increased in the BAT of SC-treated HFD mice. In addition, our *in vitro* experiments revealed that SC led to increased AMPK phosphorylation and UCP1 expression in differentiated IBA cells. Importantly, increased UCP1 expression was inhibited by siAMPK-mediated AMPK downregulation. These results clearly demonstrate AMPK activation involvement in the thermogenic function of SC in BAT.

Several *in vivo* and *in vitro* studies have shown that chronic overfeeding leads to desensitization of β-receptor mediated responses (Hausdorff et al., 1990; Lohse,

1993) and the chronic overactivity of SNS due to overfeeding has also been suggested to increase the risk of metabolic dysfunction (Thorp et al., 2015). The activation and the mechanism of the β-3 adrenergic system in BAT are not yet clear. However, since the mechanism of β-3 adrenergic system is a major mechanisms of heat production, it is necessary to further study whether SC affects it.

Thermogenesis by UCP1 activation is considered a natural function of BAT. However, beige adipocytes can be induced by the upregulation of UCP1 expression in WAT. In the current study, UCP1 expression was dramatically increased by SC administration in sWAT but not eWAT only in mice with HFD-induced obesity. In addition, increased AMPK activity was observed in sWAT, similar to that seen in BAT. The mechanism underlying AMPK-mediated browning remains unclear, although many related studies have been conducted. AICAR was shown to increase energy expenditure and mitochondrial content but not UCP1 expression in sWAT. Another study demonstrated that AICAR treatment induced the accumulation of brown adipocytes in the WAT of mice, whereas a separate study reported that AICAR treatment in adipocytes led to increases in the protein levels of UCP1, PRDM16, and PGC1α. It was reportedly responsible for adipocyte browning, which was blocked by the AMPK inhibitor, compound C, in differentiated 3T3-L1 cells. In the present study, UCP1 protein expression was observed in differentiated adipocytes treated with SC, and the effect was decreased by AMPK siRNA transfection. These results considered that SC seems to increase the browning of white adipocyte by the activation of the AMPK mechanism in adipocytes.

SC contains active ingredients reported to activate AMPK, such as sauchinone,

quercetin, and chlorogenic acid. Several studies have reported its effects on inhibiting lipogenesis, muscle mitochondrial biogenesis, and improving blood lipids, but there have been no reports related to increased heat production. Therefore, there is a need to carry out the separation of the active compounds that contribute to heat generation through the activation of AMPK, and its efficacy and mechanisms.

Many anti-obesity drugs are not clinically applicable because of toxicity. SC has long been used as a traditional medicinal product, but, it is necessary to examine whether weight loss in animals with HFD-induced obesity that received SC treatment is caused by toxicity. In the current study, both the HFD and LFD groups were orally administered SC. In addition, there were no significant differences in body weight, body fat mass, lean mass, or biochemical markers between the LFD-vehicle and LFD-SC-100 groups. These results suggest that the improvement in obesity by SC administration is not caused by toxicity. Verification of *S. chinensis*-mediated anti-obesity effects through heat generation will contribute to the development of a new natural anti-obesity therapeutic agent.

Conclusion

The SC inhibited lipid accumulation and adipogenesis in 3T3-L1 cells and decreased body weight and fat accumulation in mice with HFD-induced obesity. Furthermore, the SC enhanced the energy expenditure and heat production as well as the thermogenesis-associated gene expression. Furthermore, AMPK activation was an underlying mechanism of the anti-obesity effect of the SC. These data provide new insights into the regulation of BAT function by a natural herb and further evidence for the potential of SC as a therapeutic strategy for the prevention and treatment of obesity and related diseases.

References

1. Singla P, Bardoloi A, Parkash A A. Metabolic effects of obesity: A review. *World J Diabetes, 1*(3), (2010). 76-88.
2. 2. Jung U J, Choi M S. Obesity and its metabolic complications: the role of adipokines and the relationship between obesity, inflammation, insulin resistance, dyslipidemia and nonalcoholic fatty liver disease. *Int J Mol Sci, 15*(4), (2014). 6184-6223.
3. Abdelaal M, le Roux C W, Docherty N G. Morbidity and mortality associated with obesity. *Ann Transl Med, 5*(7), (2017). 161.
4. OECD. Obesity update 2017, information accessed at : www.oecd.org/health/obesity-update.htm
5. Coelho M, Oliveira T, Fernandes R. Biochemistry of adipose tissue: an endocrine organ. *Arch Med Sci, 9*(2), (2013). 191-200.
6. Luo L, Liu M. Adipose tissue in control of metabolism. *J Endocrinol, 231*(3), (2016). R77-R99.
7. Gregoire F M, Smas C M, Sul H S. Understanding adipocyte differentiation. *Physiol Rev, 78*(3), (1998). 783-809.
8. Wong R H, Sul H S. Insulin signaling in fatty acid and fat synthesis: a transcriptional perspective. *Curr Opin Pharmacol, 10*(6), (2010). 684-691.
9. Terry R B, Stefanick M L, Haskell W L, Wood P D. Contributions of regional adipose tissue depots to plasma lipoprotein concentrations in overweight men and women: possible protective effects of thigh fat. *Metabolism, 40*(7), (1991). 733-740.
10. Inoue M, Maehata E, Yano M, Taniyama M, Suzuki S. Correlation

between the adiponectin-leptin ratio and parameters of insulin resistance in patients with type 2 diabetes. *Metabolism, 54*(3), (2005). 281-286.

11. Vazquez-Vela M E, Torres N, Tovar A R. White adipose tissue as endocrine organ and its role in obesity. *Arch Med Res, 39*(8), (2008). 715-728.
12. McArdle M A, Finucane O M, Connaughton R M, McMorrow A M, Roche H M. Mechanisms of obesity-induced inflammation and insulin resistance: insights into the emerging role of nutritional strategies. *Front Endocrinol (Lausanne), 4,* (2013). 52.
13. Hotamisligil G S, Arner P, Caro J F, Atkinson R L, Spiegelman B M. Increased adipose tissue expression of tumor necrosis factor-alpha in human obesity and insulin resistance. *J Clin Invest, 95*(5), (1995). 2409-2415.
14. Fasshauer M, Klein J, Lossner U, Paschke R. Interleukin (IL)-6 mRNA expression is stimulated by insulin, isoproterenol, tumour necrosis factor alpha, growth hormone, and IL-6 in 3T3-L1 adipocytes. *Horm Metab Res, 35*(3), (2003). 147-152.
15. Jager J, Gremeaux T, Cormont M, Le Marchand-Brustel Y, Tanti J F. Interleukin-1beta-induced insulin resistance in adipocytes through down-regulation of insulin receptor substrate-1 expression. *Endocrinology, 148*(1), (2007). 241-251.
16. Fujisaka S, et al. Regulatory mechanisms for adipose tissue M1 and M2 macrophages in diet-induced obese mice. *Diabetes, 58*(11), (2009). 2574-2582.

17. Lee P, Swarbrick M M, Ho K K. Brown adipose tissue in adult humans: a metabolic renaissance. *Endocr Rev, 34*(3), (2013). 413-438.
18. Timmons J A, et al. Myogenic gene expression signature establishes that brown and white adipocytes originate from distinct cell lineages. *Proc Natl Acad Sci U S A, 104*(11), (2007). 4401-4406.
19. Zhang C, et al. Inhibition of myostatin protects against diet-induced obesity by enhancing fatty acid oxidation and promoting a brown adipose phenotype in mice. *Diabetologia, 55*(1), (2012). 183-193.
20. Cypess A M, et al. Identification and importance of brown adipose tissue in adult humans. *N Engl J Med, 360*(15), (2009). 1509-1517.
21. van Marken Lichtenbelt W D, et al. Cold-activated brown adipose tissue in healthy men. *N Engl J Med, 360*(15), (2009). 1500-1508.
22. Virtanen K A, et al. Functional brown adipose tissue in healthy adults. *N Engl J Med, 360*(15), (2009). 1518-1525.
23. Wu J, Cohen P, Spiegelman B M. Adaptive thermogenesis in adipocytes: is beige the new brown? *Genes Dev, 27*(3), (2013). 234-250.
24. Bordicchia M, et al. Cardiac natriuretic peptides act via p38 MAPK to induce the brown fat thermogenic program in mouse and human adipocytes. *J Clin Invest, 122*(3), (2012). 1022-1036.
25. Guerra C, Roncero C, Porras A, Fernandez M, Benito M. Triiodothyronine induces the transcription of the uncoupling protein gene and stabilizes its mRNA in fetal rat brown adipocyte primary cultures. *J Biol Chem, 271*(4), (1996). 2076-2081.
26. Tseng Y H, et al. New role of bone morphogenetic protein 7 in brown

adipogenesis and energy expenditure. *Nature, 454*(7207), (2008). 1000-1004.

27. Coskun T, et al. Fibroblast growth factor 21 corrects obesity in mice. *Endocrinology, 149*(12), (2008). 6018-6027.
28. Puigserver P, Vazquez F, Bonet M L, Pico C, Palou A. In vitro and in vivo induction of brown adipocyte uncoupling protein (thermogenin) by retinoic acid. *Biochem J, 317 (Pt 3),* (1996). 827-833.
29. Falcou R, Bouillaud F, Mory G, Apfelbaum M, Ricquier D. Increase of uncoupling protein and its mRNA in brown adipose tissue of rats fed on 'cafeteria diet'. *Biochem J, 231*(1), (1985). 241-244.
30. Trayhurn P. Origins and early development of the concept that brown adipose tissue thermogenesis is linked to energy balance and obesity. *Biochimie, 134*, (2017). 62-70.
31. Cannon B, Nedergaard J. Brown adipose tissue: function and physiological significance. *Physiol Rev, 84*(1), (2004). 277-359.
32. Lizcano F, Vargas D. Biology of Beige Adipocyte and Possible Therapy for Type 2 Diabetes and Obesity. *Int J Endocrinol, 2016*, (2016). 9542061.
33. Cui X B, Chen S Y. White adipose tissue browning and obesity. *J Biomed Res, 31*(1), (2016). 1-2.
34. Thoonen R, Hindle A G, Scherrer-Crosbie M. Brown adipose tissue: The heat is on the heart. *Am J Physiol Heart Circ Physiol, 310*(11), (2016). H1592-1605.
35. Dalgaard L T, Pedersen O. Uncoupling proteins: functional characteristics and role in the pathogenesis of obesity and Type II diabetes. *Diabetologia,*

44(8), (2001). 946-965.

36. Brondani L A, Assmann T S, Duarte G C, Gross J L, Canani L H, Crispim D. The role of the uncoupling protein 1 (UCP1) on the development of obesity and type 2 diabetes mellitus. *Arq Bras Endocrinol Metabol*, *56*(4), (2012). 215-225.
37. Puigserver P, Wu Z, Park C W, Graves R, Wright M, Spiegelman B M. A cold-inducible coactivator of nuclear receptors linked to adaptive thermogenesis. *Cell*, 92(6), (1998). 829-839.
38. Wu Z, et al. Mechanisms controlling mitochondrial biogenesis and respiration through the thermogenic coactivator PGC-1. *Cell*, 98(1), (1999). 115-124.
39. Liang H, Ward W F. PGC-1alpha: a key regulator of energy metabolism. *Adv Physiol Educ*, 30(4), (2006). 145-151.
40. Seale P, et al. Prdm16 determines the thermogenic program of subcutaneous white adipose tissue in mice. *J Clin Invest*, 121(1), (2011). 96-105.
41. Villanueva C J, et al. Adipose subtype-selective recruitment of TLE3 or Prdm16 by PPARgamma specifies lipid storage versus thermogenic gene programs. *Cell Metab*, 17(3), (2013). 423-435.
42. Stapleton D, et al. AMP-activated protein kinase isoenzyme family: subunit structure and chromosomal location. *FEBS Lett*, *409*(3), (1997). 452-456.
43. Hawley S A, et al. Characterization of the AMP-activated protein kinase kinase from rat liver and identification of threonine 172 as the major site at

which it phosphorylates AMP-activated protein kinase. *J Biol Chem, 271*(44), (1996). 27879-27887.

44. Stapleton D, et al. Mammalian AMP-activated protein kinase subfamily. *J Biol Chem, 271*(2), (1996). 611-614.
45. Hudson E R, et al. A novel domain in AMP-activated protein kinase causes glycogen storage bodies similar to those seen in hereditary cardiac arrhythmias. *Curr Biol, 13*(10), (2003). 861-866.
46. Scott J W, et al. CBS domains form energy-sensing modules whose binding of adenosine ligands is disrupted by disease mutations. *J Clin Invest, 113*(2), (2004). 274-284.
47. Towler M C, Hardie D G. AMP-activated protein kinase in metabolic control and insulin signaling. *Circ Res, 100*(3), (2007). 328-341.
48. Kim J, Yang G, Kim Y, Kim J, Ha J. AMPK activators: mechanisms of action and physiological activities. *Exp Mol Med, 48*, (2016). e224.
49. Park H, et al. Coordinate regulation of malonyl-CoA decarboxylase, sn-glycerol-3-phosphate acyltransferase, and acetyl-CoA carboxylase by AMP-activated protein kinase in rat tissues in response to exercise. *J Biol Chem, 277*(36), (2002). 32571-32577.
50. Sullivan J E, Brocklehurst K J, Marley A E, Carey F, Carling D, Beri R K. Inhibition of lipolysis and lipogenesis in isolated rat adipocytes with AICAR, a cell-permeable activator of AMP-activated protein kinase. *FEBS Lett, 353*(1), (1994). 33-36.
51. Matejkova O, et al. Possible involvement of AMP-activated protein kinase in obesity resistance induced by respiratory uncoupling in white fat. *FEBS*

Lett, 569(1-3), (2004). 245-248.

52. Lopez M, Tena-Sempere M. Estradiol effects on hypothalamic AMPK and BAT thermogenesis: A gateway for obesity treatment? *Pharmacol Ther, 178*, (2017). 109-122.
53. van Dam A D, Kooijman S, Schilperoort M, Rensen P C, Boon M R. Regulation of brown fat by AMP-activated protein kinase. *Trends Mol Med, 21*(9), (2015). 571-579.
54. Martinez de Morentin P B, et al. Nicotine induces negative energy balance through hypothalamic AMP-activated protein kinase. *Diabetes, 61*(4), (2012). 807-817.
55. Zhang Z, et al. Berberine activates thermogenesis in white and brown adipose tissue. *Nat Commun, 5*, (2014). 5493.
56. Doan K V, et al. Gallic acid regulates body weight and glucose homeostasis through AMPK activation. *Endocrinology, 156*(1), (2015). 157-168.
57. Geerling J J, et al. Metformin lowers plasma triglycerides by promoting VLDL-triglyceride clearance by brown adipose tissue in mice. *Diabetes, 63*(3), (2014). 880-891.
58. Alberdi G, Rodriguez V M, Miranda J, Macarulla M T, Churruca I, Portillo M P. Thermogenesis is involved in the body-fat lowering effects of resveratrol in rats. *Food Chem, 141*(2), (2013). 1530-1535.
59. Corton J M, Gillespie J G, Hawley S A, Hardie D G. 5-aminoimidazole-4-carboxamide ribonucleoside. A specific method for activating AMP-activated protein kinase in intact cells? *Eur J Biochem, 229*(2), (1995).

558-565.

60. Zeqiraj E, Filippi B M, Deak M, Alessi D R, van Aalten D M. Structure of the LKB1-STRAD-MO25 complex reveals an allosteric mechanism of kinase activation. *Science, 326*(5960), (2009). 1707-1711.
61. Sakamoto K, Goransson O, Hardie D G, Alessi D R. Activity of LKB1 and AMPK-related kinases in skeletal muscle: effects of contraction, phenformin, and AICAR. *Am J Physiol Endocrinol Metab, 287*(2), (2004). E310-317.
62. Momcilovic M, Hong S P, Carlson M. Mammalian TAK1 activates Snf1 protein kinase in yeast and phosphorylates AMP-activated protein kinase in vitro. *J Biol Chem, 281*(35), (2006). 25336-25343.
63. Lim C T, Kola B, Korbonits M. AMPK as a mediator of hormonal signalling. *J Mol Endocrinol, 44*(2), (2010). 87-97.
64. Minokoshi Y, et al. Leptin stimulates fatty-acid oxidation by activating AMP-activated protein kinase. *Nature, 415*(6869), (2002). 339-343.
65. Lee Y, et al. Hyperleptinemia prevents lipotoxic cardiomyopathy in acyl CoA synthase transgenic mice. *Proc Natl Acad Sci U S A, 101*(37), (2004). 13624-13629.
66. Yamauchi T, et al. Adiponectin stimulates glucose utilization and fatty-acid oxidation by activating AMP-activated protein kinase. *Nat Med, 8*(11), (2002). 1288-1295.
67. Kola B, et al. Cannabinoids and ghrelin have both central and peripheral metabolic and cardiac effects via AMP-activated protein kinase. *J Biol Chem, 280*(26), (2005). 25196-25201.

68. Kola B, et al. The orexigenic effect of ghrelin is mediated through central activation of the endogenous cannabinoid system. *PLoS One, 3*(3), (2008). e1797.

69. Lee A Y, Han Y A, Kim J E, Hong S H, Park E J, Cho M H. Saururus chinensis Baill induces apoptosis through endoplasmic reticulum stress in HepG2 hepatocellular carcinoma cells. *Food Chem Toxicol, 83*, (2015). 183-192.

70. Lee E, et al. Anti-asthmatic activity of an ethanol extract from Saururus chinensis. *Biol Pharm Bull, 29*(2), (2006). 211-215.

71. Yoo H J, Kang H J, Jung H J, Kim K, Lim C J, Park E H. Anti-inflammatory, anti-angiogenic and anti-nociceptive activities of Saururus chinensis extract. *J Ethnopharmacol, 120*(2), (2008). 282-286.

72. Quan Z, et al. Ethanol extracts of Saururus chinensis suppress ovalbumin-sensitization airway inflammation. *J Ethnopharmacol, 132*(1), (2010). 143-149.

73. Cho H Y, Cho C W, Song Y S. Antioxidative and anti-inflammatory effects of Saururus chinensis methanol extract in RAW 264.7 macrophages. *J Med Food, 8*(2), (2005). 190-197.

74. Yu M H, et al. Effects of ethanol extract from Saururus chinensis (Bour.) Baill on lipid and antioxidant metabolisms in rats fed a high-fat diet. *Nat Prod Res, 22*(3), (2008). 275-283.

75. Kim B W, et al. Attenuation of inflammatory-mediated neurotoxicity by Saururus chinensis extract in LPS-induced BV-2 microglia cells via regulation of NF-kappaB signaling and anti-oxidant properties. *BMC*

Complement Altern Med, 14, (2014). 502.

76. Kim H Y, et al. A methylene chloride fraction of Saururus chinensis induces apoptosis through the activation of caspase-3 in prostate and breast cancer cells. *Phytomedicine, 18*(7), (2011). 567-574.
77. Jeong H J, Koo B S, Kang T H, Shin H M, Jung S, Jeon S. Inhibitory effects of Saururus chinensis and its components on stomach cancer cells. *Phytomedicine, 22*(2), (2015). 256-261.
78. Wang L, et al. The hepatoprotective and antifibrotic effects of Saururus chinensis against carbon tetrachloride induced hepatic fibrosis in rats. *J Ethnopharmacol, 126*(3), (2009). 487-491.
79. Kwon R H, Ha B J. Protection of Saururus Chinensis Extract against Liver Oxidative Stress in Rats of Triton WR-1339-induced Hyperlipidemia. *Toxicol Res, 30*(4), (2014). 291-296.
80. Ryu S Y, Oh K S, Kim Y S, Lee B H. Antihypertensive, vasorelaxant and inotropic effects of an ethanolic extract of the roots of Saururus chinensis. *J Ethnopharmacol, 118*(2), (2008). 284-289.
81. Choi M S, et al. Inhibitory effects of Saururus chinensis (LOUR.) BAILL on the development of atopic dermatitis-like skin lesions in NC/Nga mice. *Biol Pharm Bull, 31*(1), (2008). 51-56.
82. Yun Y R, et al. Lipid-lowering effect of hot water-soluble extracts of Saururus chinensis Bail on rats fed high fat diets. *J Med Food, 10*(2), (2007). 316-322.
83. Li N, et al. Two new lignans from Saururus chinensis and their DGAT inhibitory activity. *Fitoterapia, 101*, (2015). 46-50.

84. Li C, Li N, Yue J, Song Q, Fan Q. Two new lignans from Saururus chinensis. *Nat Prod Res, 31*(14), (2017). 1598-1603.
85. Kim Y W, et al. Efficacy of sauchinone as a novel AMPK-activating lignan for preventing iron-induced oxidative stress and liver injury. *Free Radic Biol Med*, 47(7), (2009). 1082-1092.
86. Kim Y W, et al. Inhibition of SREBP-1c-mediated hepatic steatosis and oxidative stress by sauchinone, an AMPK-activating lignan in Saururus chinensis. *Free Radic Biol Med*, 48(4), (2010). 567-578.
87. Kim Y W, Jang E J, Kim C H, Lee J H. Sauchinone exerts anticancer effects by targeting AMPK signaling in hepatocellular carcinoma cells. *Chem Biol Interact*, 261, (2017). 108-117.
88. Daneschvar H L, Aronson M D, Smetana G W. FDA-Approved Anti-Obesity Drugs in the United States. *Am J Med, 129*(8), (2016). 879 e871-876.
89. Thielecke F, Boschmann M. The potential role of green tea catechins in the prevention of the metabolic syndrome - a review. *Phytochemistry, 70*(1), (2009). 11-24.
90. Herranz-Lopez M, et al. Multi-Targeted Molecular Effects of Hibiscus sabdariffa Polyphenols: An Opportunity for a Global Approach to Obesity. *Nutrients, 9*(8), (2017).
91. Chuah L O, Ho W Y, Beh B K, Yeap S K. Updates on Antiobesity Effect of Garcinia Origin (-)-HCA. *Evid Based Complement Alternat Med, 2013*, (2013). 751658.
92. Chen HJ1, Li X, Chen JW, Guo S, Cai BC. Simultaneous determination of

eleven bioactive compounds in Saururus chinensis from different harvesting seasons by HPLC-DAD. *J. Pharm. Biomed Anal.* 51, (2010). 1142-1146.

93. Chen G, Goeddel D V. TNF-R1 signaling: a beautiful pathway. *Science, 296*(5573), (2002). 1634-1635.
94. Kern P A, Saghizadeh M, Ong J M, Bosch R J, Deem R, Simsolo R B. The expression of tumor necrosis factor in human adipose tissue. Regulation by obesity, weight loss, and relationship to lipoprotein lipase. *J Clin Invest, 95*(5), (1995). 2111-2119.
95. Kern P A, Ranganathan S, Li C, Wood L, Ranganathan G. Adipose tissue tumor necrosis factor and interleukin-6 expression in human obesity and insulin resistance. *Am J Physiol Endocrinol Metab, 280*(5), (2001). E745-751.
96. Aune U L, Ruiz L, Kajimura S. Isolation and differentiation of stromal vascular cells to beige/brite cells. *J Vis Exp*(73), (2013).
97. Ibrahim M M. Subcutaneous and visceral adipose tissue: structural and functional differences. *Obes Rev, 11*(1), (2010). 11-18.
98. Choi J H, Yun J W. Chrysin induces brown fat-like phenotype and enhances lipid metabolism in 3T3-L1 adipocytes. *Nutrition, 32*(9), (2016). 1002-1010.
99. Kumar P, Peers C. AMP-activated protein kinase: function and dysfunction in health and disease. *J Physiol, 574*(Pt 1), (2006). 3-6.
100. Moon H S, Chung C S, Lee H G, Kim T G, Choi Y J, Cho C S. Inhibitory effect of (-)-epigallocatechin-3-gallate on lipid accumulation of

3T3-L1 cells. *Obesity (Silver Spring), 15*(11), (2007). 2571-2582.

101. Hwang J T, et al. Genistein, EGCG, and capsaicin inhibit adipocyte differentiation process via activating AMP-activated protein kinase. *Biochem Biophys Res Commun, 338*(2), (2005). 694-699.

102. Wang S, Zhu M J, Du M. Prevention of obesity by dietary resveratrol: how strong is the evidence? *Expert Rev Endocrinol Metab, 10*(6), (2015). 561-564.

103. Wang C Y, Liao J K. A mouse model of diet-induced obesity and insulin resistance. *Methods Mol Biol, 821*, (2012). 421-433.

104. Speakman J R. Measuring energy metabolism in the mouse - theoretical, practical, and analytical considerations. *Front Physiol, 4*, (2013). 34.

105. Lowell B B, et al. Development of obesity in transgenic mice after genetic ablation of brown adipose tissue. *Nature, 366*(6457), (1993). 740-742.

106. Ghorbani M, Claus T H, Himms-Hagen J. Hypertrophy of brown adipocytes in brown and white adipose tissues and reversal of diet-induced obesity in rats treated with a beta3-adrenoceptor agonist. *Biochem Pharmacol, 54*(1), (1997). 121-131.

107. Cypess A M, Kahn C R. Brown fat as a therapy for obesity and diabetes. *Curr Opin Endocrinol Diabetes Obes, 17*(2), (2010). 143-149.

108. Shen W, et al. Acupuncture promotes white adipose tissue browning by inducing UCP1 expression on DIO mice. *BMC Complement Altern Med, 14*, (2014). 501.

109. Baba S, Jacene H A, Engles J M, Honda H, Wahl R L. CT Hounsfield

units of brown adipose tissue increase with activation: preclinical and clinical studies. *J Nucl Med, 51*(2), (2010). 246-250.

110. Brown R S, Leung J Y, Kison P V, Zasadny K R, Flint A, Wahl R L. Glucose transporters and FDG uptake in untreated primary human non-small cell lung cancer. *J Nucl Med, 40*(4), (1999). 556-565.

111. Festuccia W T, Blanchard P G, Deshaies Y. Control of Brown Adipose Tissue Glucose and Lipid Metabolism by PPARgamma. *Front Endocrinol (Lausanne), 2*, (2011). 84.

112. Bartelt A, et al. Brown adipose tissue activity controls triglyceride clearance. *Nat Med, 17*(2), (2011). 200-205.

113. Vallerand A L, Perusse F, Bukowiecki L J. Cold exposure potentiates the effect of insulin on in vivo glucose uptake. *Am J Physiol, 253*(2 Pt 1), (1987). E179-186.

114. Townsend K L, Tseng Y H. Brown fat fuel utilization and thermogenesis. *Trends Endocrinol Metab, 25*(4), (2014). 168-177.

115. Luo B, et al. Chronic hexosamine flux stimulates fatty acid oxidation by activating AMP-activated protein kinase in adipocytes. *J Biol Chem, 282*(10), (2007). 7172-7180.

116. Orci L, et al. Rapid transformation of white adipocytes into fat-oxidizing machines. *Proc Natl Acad Sci U S A, 101*(7), (2004). 2058-2063.

117. Gaidhu M P, et al. Prolonged AICAR-induced AMP-kinase activation promotes energy dissipation in white adipocytes: novel mechanisms integrating HSL and ATGL. *J Lipid Res, 50*(4), (2009). 704-715.

118. Ahmadian M, et al. Desnutrin/ATGL is regulated by AMPK and is

required for a brown adipose phenotype. *Cell Metab, 13*(6), (2011). 739-748.

119. Wang S, et al. Resveratrol enhances brown adipocyte formation and function by activating AMP-activated protein kinase (AMPK) alpha1 in mice fed high-fat diet. *Mol Nutr Food Res, 61*(4), (2017).

120. Hausdorff W P, Caron M G, Lefkowitz R J. Turning off the signal: desensitization of beta-adrenergic receptor function. *FASEB J, 4*(11), (1990). 2881-2889.

121. Lohse M J. Molecular mechanisms of membrane receptor desensitization. *Biochim Biophys Acta, 1179*(2), (1993). 171-188.

122. Thorp A A, Schlaich M P. Relevance of Sympathetic Nervous System Activation in Obesity and Metabolic Syndrome. *J Diabetes Res, 2015*, (2015). 341583.

삼백초 추출물의 에너지 소비 증가를 통한 항 비만 효능연구

이 지 혜

충남대학교 대학원 약학과 생물약학전공

(지도교수 김 상 겸)

에너지 소비와 공급의 불균형은 비만의 가장 주요한 원인으로 지목된다. 현재 에너지 공급을 줄이기 위한 다양한 식욕억제제가 처방되고 있으나, 심각한 부작용으로 사용이 제한적이다. 갈색지방 활성화를 통한 에너지 소비증가는 비만 관련 대사 질환의 예방과 치료를 위한 새로운 표적으로 떠오르고 있으며 ＵＣＰ１의 활성화와 마이토콘드리아 생합성 증가는 갈색지방 활성화와 백색지방의 베이지화를 나타내는 중요한 지표로 여겨지고 있다.

삼백초는 전통의학에서 염증관련 질환을 치료하기 위한 처방의 구성약제로 사용되어왔으며, 암, 고혈압, 혈관성 질환 등 다양한 질환에 대한 효능 및 기전 연구가 활발히 이루어지고 있다. 최근 지방세포와 간세포에 대한 지방생성 억제 효능이 보고되어 삼백초의 비만치료제로서의 가능성이 제시되고

있으나, 그 기전 연구는 미비하다. 이에 본 연구는 삼백초의 비만증 개선 효능을 갈색지방 활성화 및 지방생성억제 두 가지 측면에서 규명하고자 하였다. 이를 위하여 고지방식이 및 저지방 식이를 공급받는 각각의 동물에 삼백초 추출물을 투여하였고, 고지방식이를 공급받은 동물은 삼백초 추출물을 투여하였을 때 체중증가와 체지방량이 유의하게 감소하였으나 저지방식이를 공급받는 동물에서는 체중감소가 나타나지 않아 삼백초 추출물의 항 비만 효능을 확인 할 수 있었다. 또한, 삼백초 추출물을 투여한 동물에서는 고지방식이로 인해 유발되는 이상지질혈증, 인슐린 저항성, 지방간, 조직 내 염증도 개선됨이 관찰 되었다. 삼백초 추출물을 투여한 동물에서 사료섭취와 활동 정도의 변화는 관찰되지 않았으나, 열 발생과 에너지 소비증가와 관련된 ^{18}F-FDG uptake, 열 발생 정도와 산소소비량은 유의하게 증가하였다. 또한 갈색 지방 및 백색지방에서 UCP1 과 AMPK 인산화가 유의하게 증가함이 관찰되었다.

기전 연구를 위하여 3T3-L1 분화세포에 삼백초 추출물을 처리한 결과, 삼백초 추출물이 3T3-L1 세포의 지방생성을 억제하였으며, 초기 AMPK 기전을 활성화 시킴을 확인하였다. 그리고 분화된 3T3-L1 지방세포와 iBAT 세포에 삼백초 추출물을 처리한 결과, 삼백초 추출물은 낮은 농도에서도 AMPK를 인산화하였으며 UCP1 발현을 증가시켰다. 본 연구에서는 삼백초 추출물 처리로 인한 AMPK 활성화가 지방생성억제 및 열 발생 증가에 직접적인 영향을 미쳤는지 알아보기 위하여, siAMPK를 transfection 시킨 세포에 삼백초 추출물을 처리하였다. 그 결과, 삼백초 추출물 처리로 인한 지방생성억제 효능과 UCP1의 발현증가는 AMPK 활성을 억제하면 감소하여 삼백초 추출물의 효능이 AMPK 활성과

직접적인 상관이 있음을 관찰하였다. 결과적으로 본 연구에서는 삼백초 추출물 보충이 지방생성억제 및 열 발생 증가로 비만을 억제함을 확인하였고, AMPK 활성화는 삼백초 추출물의 효능발현에 주요한 영향을 미침을 확인하였다.

또한 실험동물의 혈액에서 독성지표인 UREA, Creatinine 수치는 삼백초 투여로 인한 유의한 변화가 없었고, AST, ALT, LDH 는 오히려 비만 유발군과 비교하여 유의하게 감소하였다. 이러한 연구를 바탕으로 삼백초는 새로운 천연물 비만치료제로서 유효하게 활용될 가능성을 제시한다.

ABSTRACT*

Anti-obesity effects of *Saururus chinensis* extract through enhancing energy expenditure

Ji-Hye Lee

Department of Pharmacy, Graduate School
Chungnam National University
Daejon, Korea

(Supervised by Professor Sang Kyum Kim)

The disparity in energy consumption and supply is the main cause of obesity. Various appetite suppressants have been prescribed to

* A **dissertation** submitted to the committee of Graduate School, Chungnam National University in a partial fulfillment of the requirements for the degree of Doctor of Pharmaceutical Sciences conferred in February 2018

reduce energy supply, but their use is limited due to serious side effects. Recently, activating brown adipocyte for increase energy expenditure has emerged as a new target for the prevention and treatment of obesity-related metabolic diseases. *Saururus chinensis* (SC) is a component of traditional medicine to treat inflammation-related diseases. The pharmacological effect of SC has been reported as an anti-obesity effect, but research on its mechanism is insufficient. In this study, we sought to investigate the effect of SC on the improvement of energy expenditure by thermogenesis of brown fat and inhibition of lipogenesis of white adipocyte. To investigate the effect of SC on anti-obesity, SC was administered to each animal fed either high-fat diet (HFD) or low-fat diet (LFD), and weight gain and fat mass were measured. SC administered mice decreased body weight gain and fat mass and improved dyslipidemia, insulin resistance, fatty liver, and inflammation caused by HFD. To determine the effect of SC extract on heat production and energy

expenditure, 18^{F}-FDG uptake and heat and oxygen consumption were measured before the autopsy and the gene and protein expression related to thermogenesis were measured. Findings showed was no change in food intake and activity level due to SC administration, but the oxygen uptake and thermogenesis were significantly increased in SC-administered HFD-fed mice compared to HFD-fed mice without SC. Phospho AMPK and UCP1 expression were significantly increased in SC administered HFD-fed mice compared to HFD-fed mice without SC. To investigate the effect of SC on lipogenesis, 3T3-L1 cells were treated with SC. As a result, SC inhibited lipogenesis of 3T3-L1 cells and activated early stage of AMPK mechanism. In particular, in order to investigate whether AMPK activation of SC directly affected lipogenesis inhibition and activate UCP1, SC was treated to siAMPK transfected 3T3-L1 adipocytes and iBAT cells. It was found that SC increased phospho AMPK and inhibited lipogenesis in 3T3-L1 cells and increased UCP1 expression in iBAT cells. Especially, the

inhibitory effect of SC on lipogenesis and the increase of UCP1 expression decreased with inhibition of AMPK activity. As a result, in this study, it was observed that supplementation of SC extract inhibited obesity by inhibiting lipogenesis in white adipocytes and increasing energy consumption by thermogenesis. It was also observed that AMPK activation had a major effect on the expression of SC. In addition, UREA and creatinine levels, which are toxic indicators, were not significantly changed by SC administration, and AST, ALT, and LDH were significantly decreased compared with the obese group. Based on these studies, SC is suggested to be used effectively as a new natural product obesity treatment.